Chapter 5

Role of Trimetallic Catalysts in Steam Methane Reforming

5.1 Role of trimetallic catalyst Ni-Fe-La/Al_2O_3

5.1.1. Introduction

The major challenge in steam methane reforming is high CO content which can damage PEM fuel cell. Therefore, the CO content can be reduced if water gas shift reaction (WGS) is promoted. However, WGS is favored at low temperature. Hence, to reduce the CO selectivity it is critical to synthesize a low temperature SMR catalyst. Another major concern of high temperature SMR operation is catalyst deactivation due to coking [1-3]. To avoid the coking problem, noble metal catalysts are commonly used for SMR process [4-5]. However, high cost of noble metal makes such catalyst commercially unsympathetic. Nickel based catalysts have found more attention in the literature for SMR process due to its low cost [6,7]. However, methane adsorbed on the Nickel catalyst make a Ni-C bond which leads to deactivation of the catalyst [8]. Hence, Nickel is generally mixed with another metal and several researchers have worked on bimetallic catalysts to improve the performance of the Nickel based catalyst [9-11]. Further, several works are reported on effect of support on performance of Nickel based catalyst for SMR process [12-13] Effect of promoters on SMR performance is also studied by many researchers [9,14-15]. Rhodium and Ruthenium are used to minimize the coking as they generate amorphous carbon [16-17]. Iron and Lanthanum are used in dry reforming to reduce the CO selectivity [9,15,18-21]. Baudh et al. [9] have reported that Lanthanum and Iron promoted Ni catalyst supported on alumina shows high catalytic activity towards steam methane reforming by reducing the CO selectivity.

In the current work, the performance of Lanthanum and Iron promoted Nickel based trimetallic catalysts supported alumina are investigated for SMR process targeting the membrane reformer application with a wish list of: low CO selectivity, low temperature operation and low startup time (low response time). The synthesized catalysts are characterized with various techniques such as SEM (Scanning electron microscope), TEM (Transmission electron microscope), XRD (X-ray diffraction), XPS (X-ray photoelectron microscopy), BET (Brunauer Emmett Teller), FTIR (Fourier transform infrared spectroscopy). The performance of the catalyst is tested in a packed bed reactor by varying temperature, W/F ratio, and total metal loading. Finally, the performance of best catalyst is tested for long term operation.

Table 5.1 Literature survey

Study	Catalyst	Remarks	Author
Performance of Ni-Based Catalysts with La Promoter for the Dry Reforming of Methane	Ni-based catalysts with La promoter	La addition improved catalyst stability and resistance to carbon deposition in methane reforming reactions.	Chen et al., 2024 [31]
Role of Fe Species of Ni-Based Catalysts for Efficient Low Temperature Ethanol Steam Reforming	Ni–Fe catalysts with varying Fe species	Different iron species influenced methane suppression in ethanol steam reforming, suggesting potential implications for steam methane reforming.	Wu et al., 2021 [28]

Bimetallic Ni Fe Nanoparticles Supported on CeO_2 as Catalysts for Steam methane reforming	Ni-Fe/CeO_2 catalysts	Ni-Fe nanocatalysts exhibited coke-resistant properties in steam methane reforming, indicating the effectiveness of bimetallic systems.	Braga et al., 2023 [11]
La-Doped Supported Ni Catalysts for Steam Reforming of Methane	Ni/Al_2O_3 catalysts doped with La	La doping enhanced Ni dispersion and improved catalyst performance in steam methane reforming.	Boudjeloud et al., 2019 [21]
Ni-Fe/$MgAl_2O_4$	Ethanol steam reforming	Notable for high ethanol conversion efficiency, with structural modifications improving catalyst performance and stability during multiple reforming cycles.	Lara et al., 2024 [22]
Ni-Fe Smart Catalysts	Dry methane reforming using in situ X-ray absorption spectroscopy	In situ X-ray absorption spectroscopy tracked dynamic structural changes, revealing insights into the activation and deactivation behavior of NiFe catalysts in dry methane reforming.	Shah et al., 2023 [23]
Ni–Fe–La Catalytic System	CO_2 utilization for sustainable syngas production	Optimized Ni–Fe–La-based catalytic system showed high CO_2 conversion efficiency,	Shah et al., 2023 [24]

	via dry reforming of methane	stable performance, and enhanced syngas production rates in dry reforming of methane.	
$LaFe_{1-x}Ni_xO_3$ Perovskites	High-temperature decomposition of nitrous oxide	$LaFe_{1-x}Ni_xO_3$ perovskites showed improved catalytic activity and stability in the high-temperature decomposition of N_2O, with Ni doping enhancing the decomposition rate.	Isupova et al., 2024 [25]
Ca-La co-doped CeO_2	Partial oxidation of methane	The Ca-La co-doping in CeO_2 enhanced catalytic activity and stability, leading to increased methane conversion and higher hydrogen selectivity under partial oxidation conditions.	Sarmad et al., 2021 [26]

The study of Ni-Fe-La/Al_2O_3 catalysts demonstrates their promising potential for steam methane reforming because of their increased catalytic activity, stability, and resistance to coke formation; lanthanum (La) is an important promoter that improves the dispersion of Ni on the catalyst support and stabilizes the active metal against sintering at high temperatures; La also helps to reduce carbon deposition, a major problem in methane reforming processes; iron (Fe), when added to Ni-based catalysts, introduces synergistic bimetallic effects that improve catalytic activity.

These studies highlight the potential benefits of incorporating La and Fe into Ni-based catalysts for methane reforming processes, including enhanced stability, resistance to carbon deposition, and improved catalytic performance.

5.2. Experimental

5.2.1. Catalyst preparation

In current work, trimetallic catalysts are synthesized for hydrogen generation using steam methane reforming that consists of a prefixed ratio of metals Ni, Fe and La loaded to alumina support. All precursors' salts supplied by Merck Chemicals. Alumina is used as a support material. The total metal loading is varied from 5 to 15wt.%. Nickel ratio is fixed to 75wt%, whereas Fe:La ratio is varied from 20:5, 15:10 and 10:15 wt.% of the total metal loading.

First , gamma alumina in powder form as a support is calcined in a muffle furnace at 970℃ temperatures at a rate of 1°C/minute for 6 hours' time to obtain the powder of theta alumina as catalyst support. Nickel nitrate hexahydrate is used as a precursor salt for nickel whereas, Iron nitrate nonahydrate and Lanthanum nitrate hexahydrate are used as precursor for iron and lanthanum metal loading respectively. All precursors are added into alumina solution with vigorous stirring at temperature 70℃. This solution is kept for 10 hours of time under vigorous stirring in a trimetallic mixture solution. The pH is maintained between 6-8 to obtain a slurry, and then this obtained slurry is kept for drying at 120°C temperature for overnight. This is followed by crushing and calcination to turn the nitrates into oxides in the presence of air at 970℃ temperature for 6 hours in a muffle furnace to obtain a trimetallic catalyst. Then this calcinated catalyst is crushed in a mortar pestle to get the desired size of 180-300 microns. The same is used for characterization and testing.

5.2.2. Catalyst characterization

XRD analysis of all the catalysts are analyzed by Rigaku XRD analyzer. The peaks in the 2-theta range of 10°-80° identified by XRD analysis with Cu-Kα radiation. The BET instrument is used to calculate the surface area, pore volume and pore diameter of the catalyst samples using N_2 adsorption-desorption isotherms. The BET results are recorded by BET instrument MESO 112®. Degassing is performed for all catalyst samples at temperature 200℃ for 2 hours to remove all the volatile impurities. BJH analysis is conducted to determine the pore size distribution of catalysts. TEM analysis is performed on Tecnai G2 20 TWIN instrument to scan the surface morphology of catalysts. To prepare the TEM sample a pinch of catalyst is suspended in ethanol and kept for sonication for at least half an hour. After that, one drop of that suspended solution is dispersed on the surface of TEM copper grid and kept for drying for 12 hours. The spent catalysts are also analyzed by TEM to identify the change in surface morphology after the reaction. FTIR analysis is carried out on Nicolet iS5® instrument. Prior to FTIR analysis, powder sample is palletized of around 1 cm without using any additives. FESEM analysis is also performed using high resolution scanning electron microscope (Nova nano SEM 450®) instrument. Powdered samples are analysed using SEM technique for the surface morphology and characteristics. Elemental compositions of catalysts are also identified using EDS analyzer. XPS characterization is done using Thermo Fisher Scientific K-alpha. Binding energy of different elements Nickel, Lanthanum and Iron are identified with XPS analysis.

5.2.3. Catalyst Test

The synthesized catalysts are tested in packed bed reactor of inner diameter of 11.74mm and 600mm length. For the SMR reaction, methane gas was injected from the reactor's top. To keep processing parameters constant, nitrogen was employed as an inert gas. The water in form of steam was also supplied from the top of the reactor. Steam was produced by a

vaporizer which was maintained at a temperature 350℃. The gas (methane and nitrogen mixture) was passed through the pre-mixer where gas is heated up to 350℃ temperatures. The catalyst was packed in the bottom section of packed bed reactor and was placed in the heated zone by using catalyst holder. The product gases H_2, CO, CO_2, inert N_2, and unconverted CH_4 and steam passed through condenser followed by a gas-liquid separator. A chilled brine solution maintained at -5 ℃ is passed through the jacket of condenser and gas-liquid separator to condense unutilized water. The outlet gas flowrate from gas-liquid separator was measured through gas flow meters. The outlet gas samples were collected in a tedlar bags after certain intervals which was analyzed by using gas chromatography. The experiments were conducted at different temperatures between 500℃ to 800℃, W/F between 12to 32 kg $_{cat}$.s. molCH_4^{-1}, and total metal doping from 5 to 15% to optimize the process conditions for synthesized trimetallic catalysts.

5.3 Results and discussion

5.3.1 Catalytic Activity

The catalytic activity of trimetallic Ni-Fe-La/Al_2O_3 catalyst is studied in packed bed reactor. The reaction is carried out at temperature range of 500-800℃ with total metal loading of varying from 5 to 15wt%. Three metal compositions 75Ni-20Fe-5La, 75Ni-15Fe-10La, and 75Ni-10Fe-15La by wt.% are tested. Initially, the metal loading for these catalysts was kept constant at 10 wt.%. Fig 5.1a shows the conversion vs temperature graph for all the metal compositions. It can be clearly seen that metal composition 75Ni-20Fe-5La shows almost 100% conversion at temperature 750 ℃ and above while the other two composition catalysts showed the same at 700 ℃. However, 75Ni-20Fe-5La gives higher conversion at low temperature compared to the other two catalysts. Therefore, the performance of all the catalysts is analyzed with the time which are presented in Fig 5.1b, 5.1c and 5.1d. The results show that all the catalysts have stable performance with the time

for 60 min. 75Ni-20Fe-5La gives maximum conversion (~30%) at 500 ℃ while 75Ni-15Fe-10La and 75Ni-10Fe-15La provide 20% and 10% conversion respectively. The increase in temperature increases the conversion for all the three catalysts. At high temperature 75Ni-15Fe-10La and 75Ni-10Fe-15La show better activity than 75Ni-20Fe-5La. All the three catalysts showed low response time (low startup time). At 700 ℃ 75Ni-15Fe-10La and 75Ni-10Fe-15La showed almost 100% conversion from 10 min (first sample collection time) to 60 min. Hence, it can be concluded that both 75Ni-15Fe-10La and 75Ni-10Fe-15La performs equally well from conversion perspective and show high catalytic activity. However, 75Ni-15Fe-10La catalyst shows higher activity at low temperature compared to 75Ni-10Fe-15La, as more content of iron promotes the water gas shift reaction by activation of steam. The low lanthanum content helps in removal of carbonaceous species [27-28]. Hydrogen atoms can move from one metal particle to another when specific metals are present, which facilitates methane activation and speeds up the reforming process. This phenomenon is known as the hydrogen spillover effect. Catalytic activity at low temperatures can be improved by this phenomenon. Moreover, lanthanum is more hazardous and costly than iron. Therefore, we have chosen metal composition 75Ni-15Fe-10La for the rest of experiments by taking care of less amount of lanthanum as compared to iron.

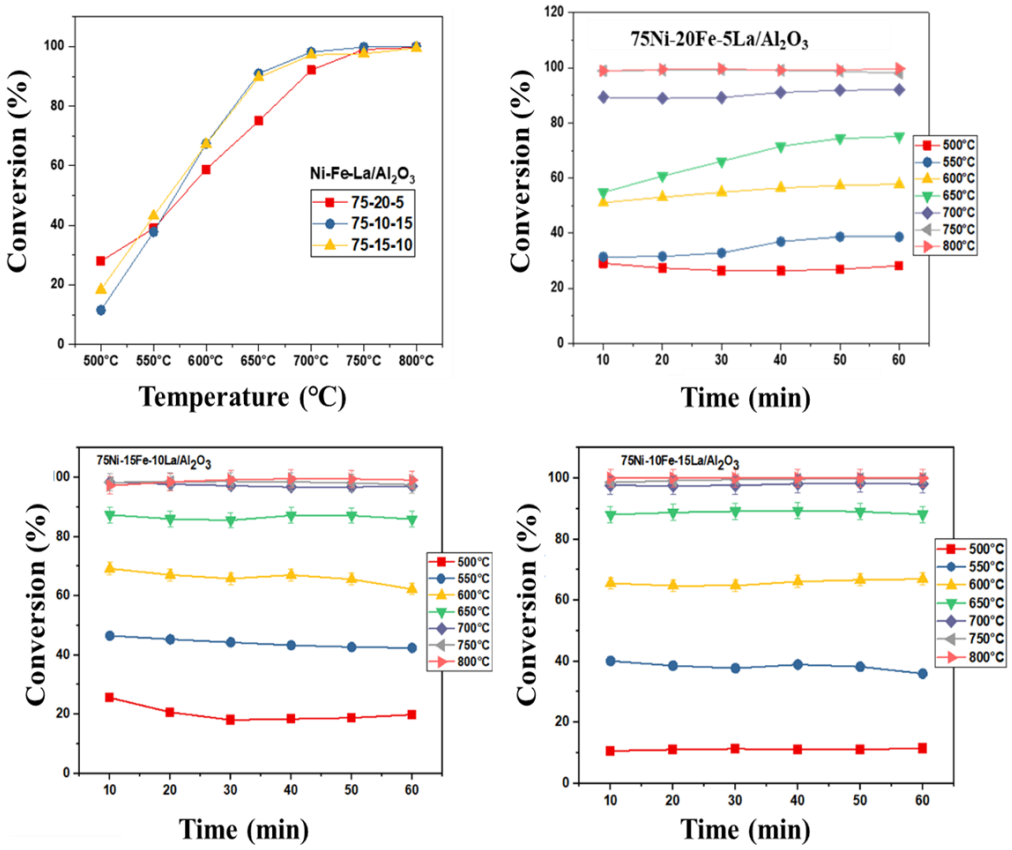

Fig. 5.1 (a) Conversion vs Temperature graph of different compositions (b) conversion vs time graph 75Ni-20Fe-5La (c) conversion vs time graph of 75Ni-15Fe-10La (d) conversion vs time graph of 75Ni-10Fe-10La

Fig 5.2 (a-d) represents the catalytic activity of 75Ni-15Fe-10La trimetallic catalyst in terms of conversion, CO selectivity, CO_2 selectivity and H_2 Yield. The CO selectivity for this trimetallic catalyst is zero at low temperature 500°C. CO selectivity is approximately 57% for higher temperature 800°C when related to CO and CO_2 only. Similarly, for CO_2 selectivity, it shows 100% CO_2 selectivity at low temperature 500°C. H_2 yield for this trimetallic catalyst is around 3.7 at temperatures above 700°C. Whereas, it also exhibits good hydrogen yield around 1.7 at lower temperature 550°C. Therefore, it can be concluded that this trimetallic catalyst can be used for the membrane reformer application as the CO selectivity is zero at low temperature, it shows low startup time and also provide stable operation upto 60 min. At higher temperature (700 °C) where the conversion is 100% it

shows higher CO_2 selectivity. Hence, it is suitable for both low temperature and moderate temperature application.

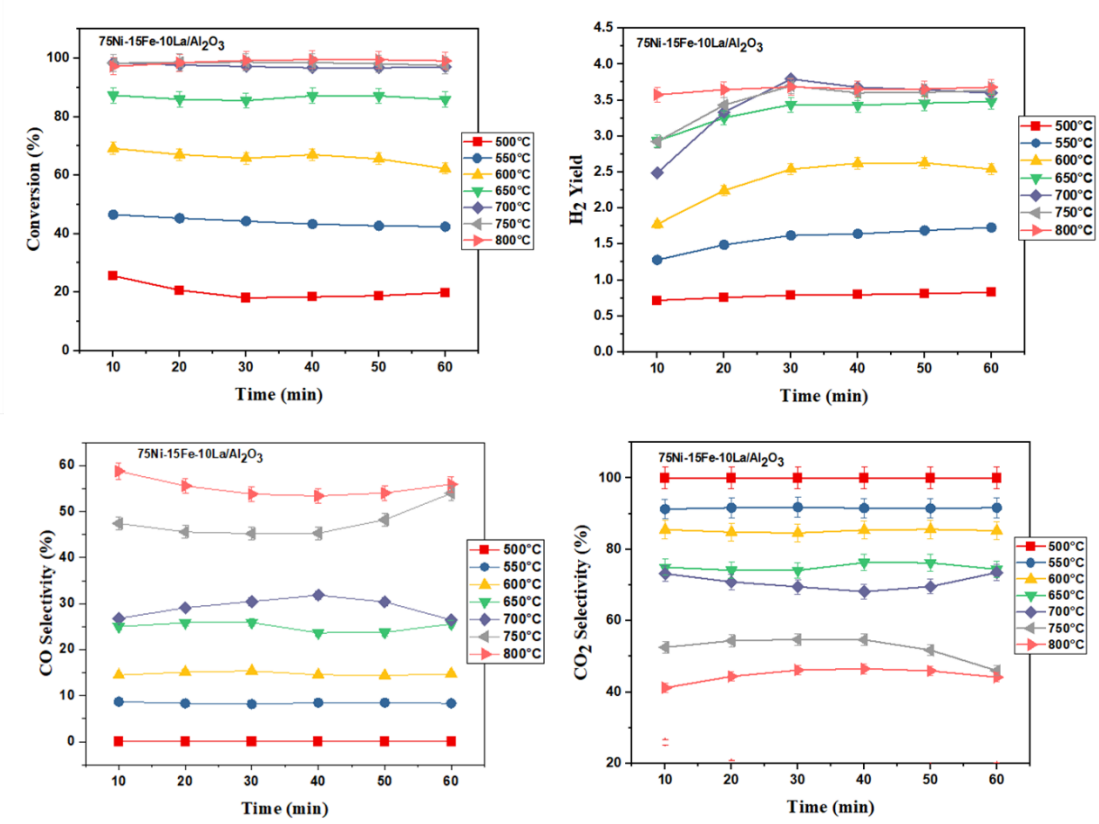

Fig. 5.2 Catalytic activity of 75Ni-15Fe-10La (a) Conversion vs time (b) H_2 yield vs time (c) CO selectivity vs time (d) CO_2 selectivity vs time

Fig 5.3 a-d show catalytic activity of 75Ni-15Fe-10La/Al_2O_3 trimetallic catalyst for all *W/F* ranges from 14-32 kg_{cat} s /mol_{CH4} to find out the optimum value of *W/F* at 700 °C. Here, *W* is the weight of the catalyst and *F* is the molar flow rate of methane input. As we go on increasing the *W/F* value from 14 to 32 kg_{cat} s /mol $_{CH4}$, conversion increases from 80% to almost 100%. It can be concluded that higher W/F represents lower flow rate of methane input which is responsible for high residence time in the reactor. Therefore, higher residence time in the reactor attributed to higher methane conversion. The term "residence time" describes how long the reactants (steam and methane) stay in contact with the

catalyst. The methane molecules have more time to interact with the catalyst's active sites as residence time grows. Longer residence times bring the system closer to thermodynamic equilibrium, when the process converts a larger amount of methane into synthesis gas (H_2 and CO) [29]. The lower W/F values reduce the conversion and increases the CO selectivity. This is mainly due to reduced concentration of CO which suppress the water gas shift reaction and leads to high CO selectivity.

CO selectivity for higher W/F at 700 ℃ is around 25% which is quite low compared to traditional reformer catalysts. Hence, the newly synthesized catalyst is promising for membrane reformer application. Further, high H_2 Yield is obtained with W/F 32 kg_{cat} s /mol_{CH4}.

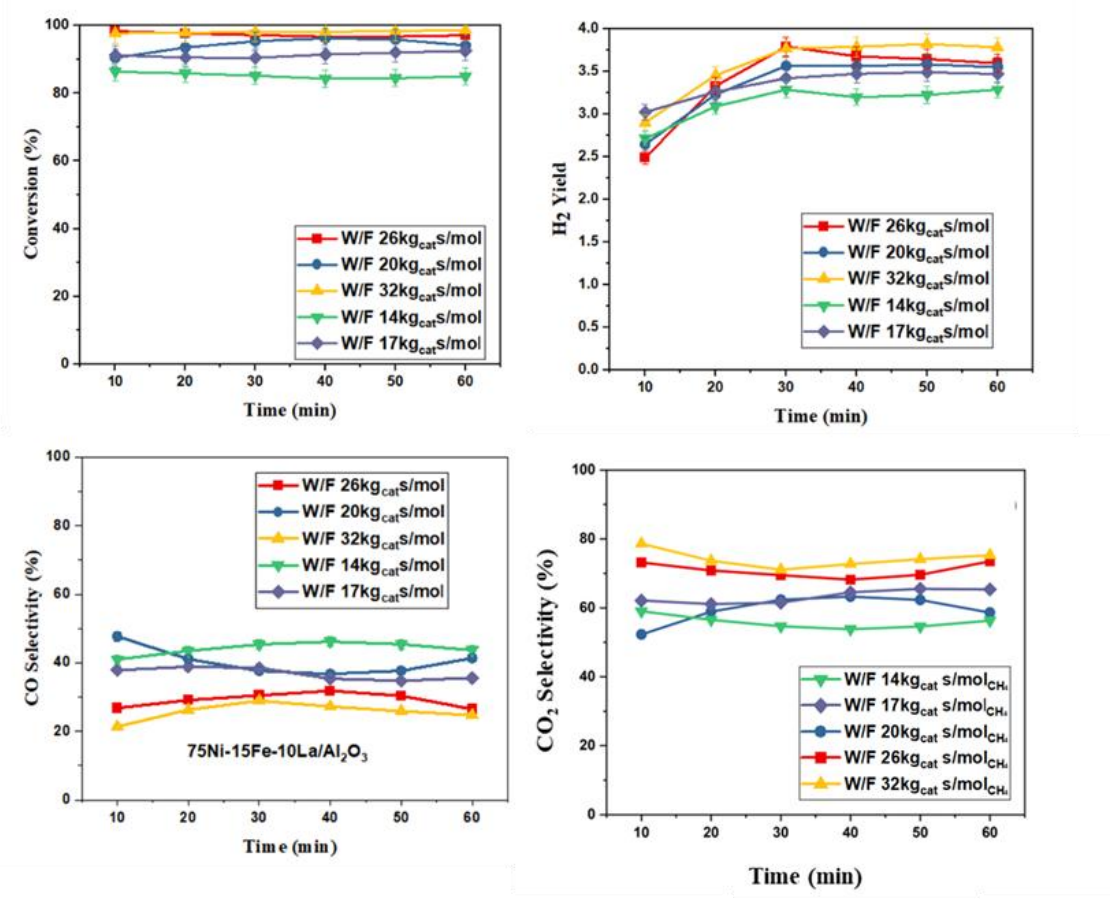

Fig. 5.3 Effect of W/F on 75Ni-15Fe-10La at 700 ℃ (a) Conversion vs time graph (b) H_2 Yield vs time (c) CO selectivity vs time (d) CO_2 selectivity vs time

Fig 5.4 represents the variation in methane conversion and hydrogen production rate with W/F values at 700 °C temperature. It is observed that with increase in W/F value, conversion is increasing due to increase in contact time. However, hydrogen production rate is reducing due to decrease in methane flow rate. It should be noted that in current experiment the amount of catalyst was kept constant and flowrate of methane was changed to vary the W/F ratio. It is found that the conversion line and hydrogen production rate cross each other at W/F 18.5 kg_{cat} s /mol_{CH4}. Therefore, optimum value of W/F for newly synthesized 75Ni-15Fe-10La on alumina catalyst is 18.5 kg_{cat}s /mol_{CH4} at 700 °C temperature.

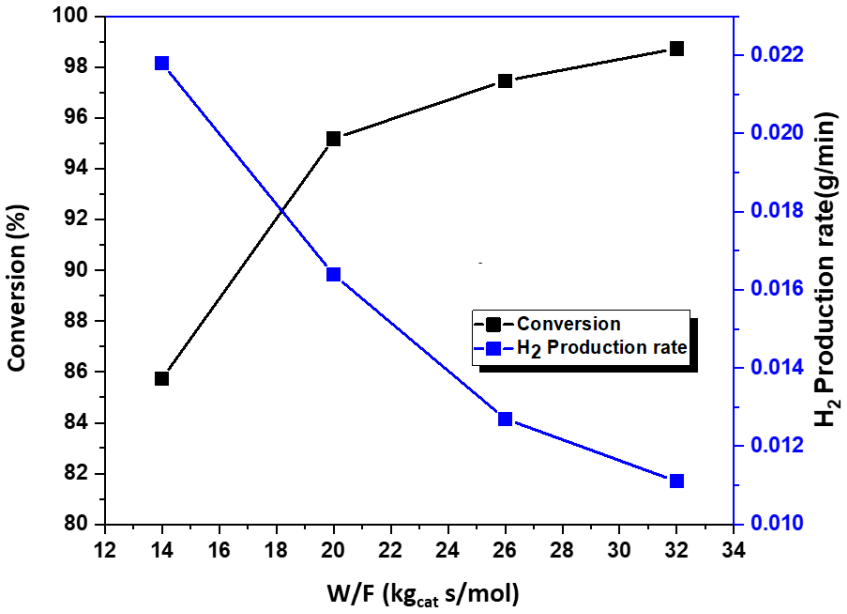

Fig. 5.4 Conversion, H_2 production rate vs W/F value for 75Ni-15Fe-10La catalyst at 700 °C

Fig 5.5 represents the effect of total metal loading of the catalyst on the conversion. The effect of total metal loading of catalyst is observed for 5%, 10% and 15% by keeping the metal composition same i.e. 75Ni-15Fe-10La . From the Fig 5.5a, conversion is increasing up to 10% and then dropping after 10% metal loading. The test of varying the total metal

loading is done at the optimum temperature 700°C, optimum W/F for this catalyst 18.5 $kg_{cat}s/mol$. The drop in conversion at 15% metal loading is due to blocking of the pores over the active surface area which is responsible for less catalytic activity. Limitations in mass transfer may also result from increasing the metal load. The removal of products (CO and H_2) and the diffusion of reactants (steam and methane) to the active sites may be impeded as the metal loading rises. This is especially true if the structure of the catalyst gets overly thick, which hinders gases ability to enter and interact with the active sites [30]. The CO selectivity is also very high (almost 55% at temperature 700°C) for metal loading 15% as compared to 5% and 10%. In comparison of 5% and 10% metal loading, hydrogen yield of 10% metal loading is high (~3.5 at temperature 700°C) as compared to 5% metal loading. Therefore, total metal loading 10% is chosen for all the experiments.

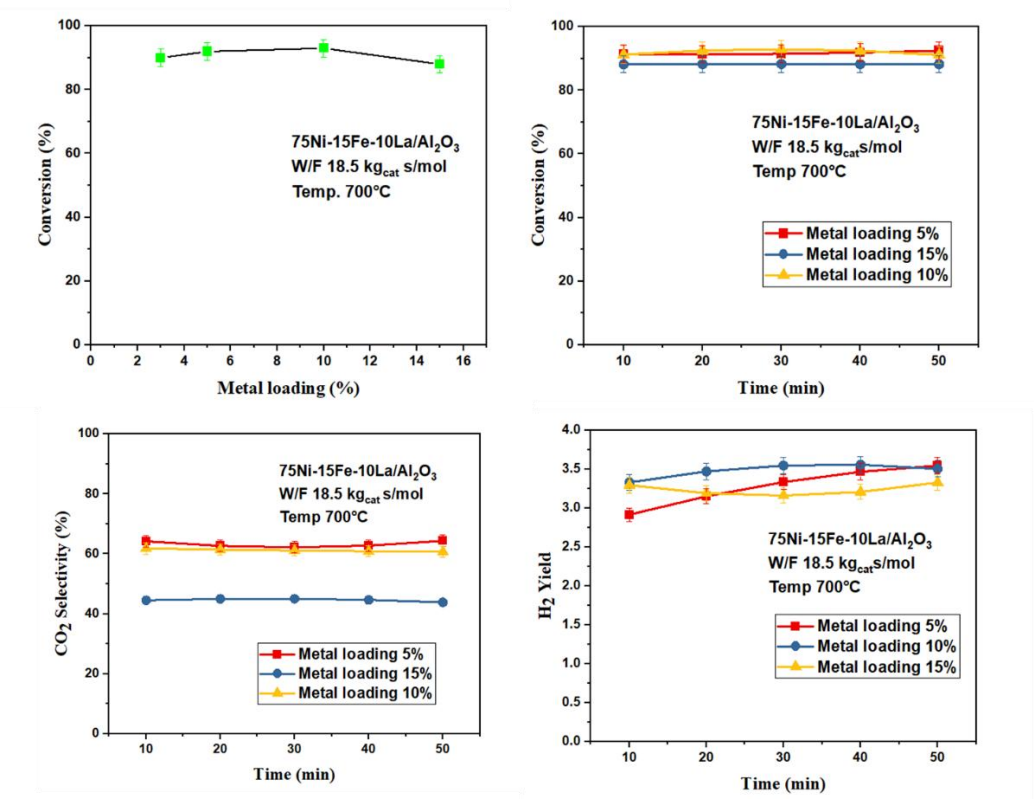

Fig. 5.5 (a) Conversion vs metal loading graph of 75Ni-15Fe-10La catalyst (b) Conversion vs time graph w.r.t metal loadings (c) CO_2 selectivity vs time graph (d) H_2 yield vs time graph

5.3.2 Long term stability test

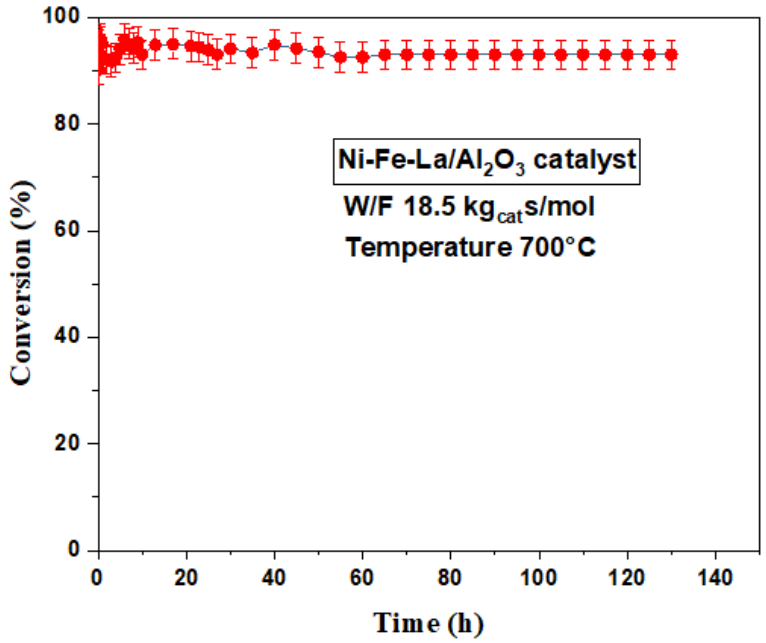

Fig. 5.6 Long term stability test of 75Ni-15Fe-10La catalyst for at least 130 hours

The trimetallic catalyst Ni-Fe-La/Al_2O_3 is highly stable for at least 130 hours as shown in Fig. 5.6. There is no deactivation of the catalyst throughout the reaction at optimum conditions W/F 18.5 $kg_{cat}s$/mol, temperature 700°C. It can be concluded that this catalyst can be used for the industrial applications. Commercially, Ni/Al_2O_3 is being used in the industries for the steam reforming of methane. But the major drawback is deactivation of catalyst with time due to coke formation. Iron and lanthanum as promoters enhance the water gas shift reaction by reducing the coke formations. A Ni-Fe alloy can be formed when nickel (Ni) and iron (Fe) are bonded. Greater resistance to sintering is offered by this alloy, which is a common problem in steam reforming as catalyst particles agglomerate and lose surface area due to high temperatures. Because of the alloy's increased thermal stability, the catalyst is more stable overall during long reaction times. In catalysts, lanthanum (La) is frequently employed as a stabilizer and promoter. It improves oxygen mobility and

makes it easier to get rid of carbon deposits, or coke, on the catalyst surface, which is one of the main reasons of steam methane reforming deactivation. Additionally, lanthanum oxides can improve the dispersion of Ni particles, extending the life of the catalyst and preserving a higher number of active sites [31].

5.3.3 Characterization results

SEM/EDS

Fig 5.7a and 5.7b represent SEM images of trimetallic catalyst 75Ni-10Fe-15La and 75Ni-15Fe-10La respectively. The SEM image of these catalysts show that metals there is no agglomeration of any material on the surface of catalyst. This may be one of the reasons of better catalytic performance of both the catalysts. According to the SEM pictures, the average particle size of the Ni and Fe clusters is estimated to be between 20 and 40 nm. The metal clusters exhibit uniform distribution across the alumina support, devoid of any indication of agglomeration. Fig 5.7c and 5.7D show the SEM images of spent 75Ni-10Fe-15La and 75Ni-15Fe-10La respectively. The images show the surface morphology of fresh and spent catalyst remains almost same. The particle size analysis of spent catalyst also shows similar particle size range as of the fresh catalyst. Hence, no agglomeration or carbon deposition is found on the catalyst after the testing. This confirms that the newly synthesized catalyst prevents the coking phenomena.

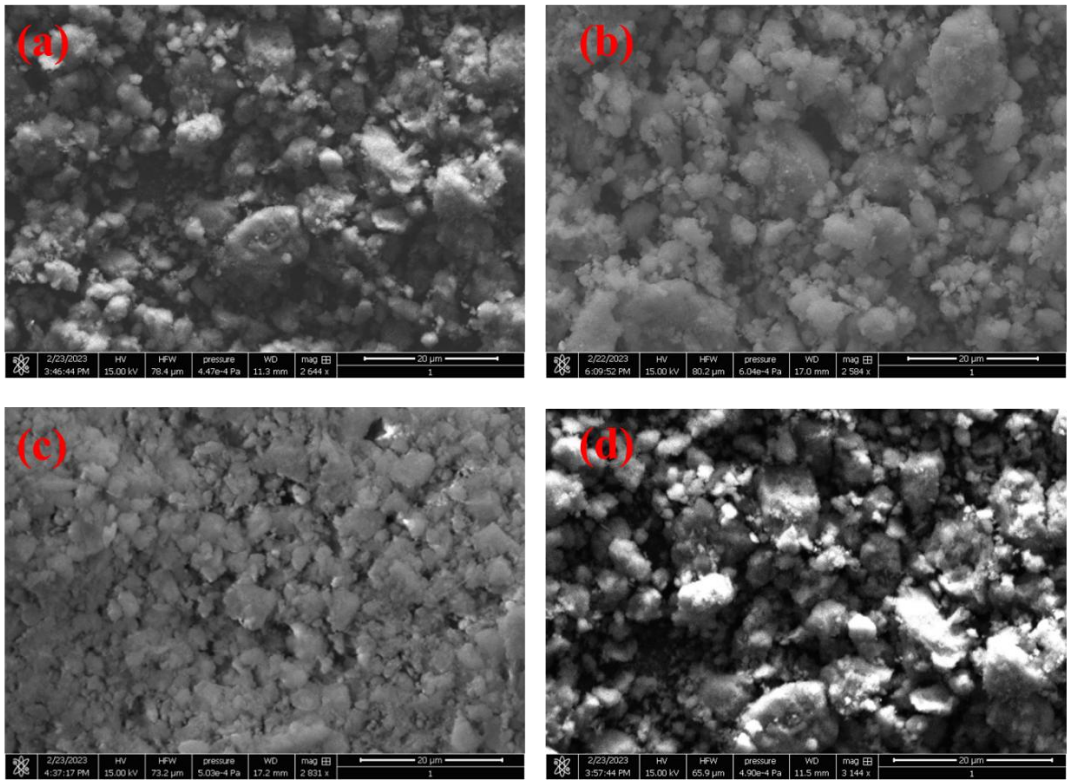

Fig. 5.7 SEM images of (a) Fresh 75Ni-10Fe-15La (b) Fresh 75Ni-15Fe-10La (c) spent 75Ni-10Fe-15La (d) 75Ni-15Fe-10La

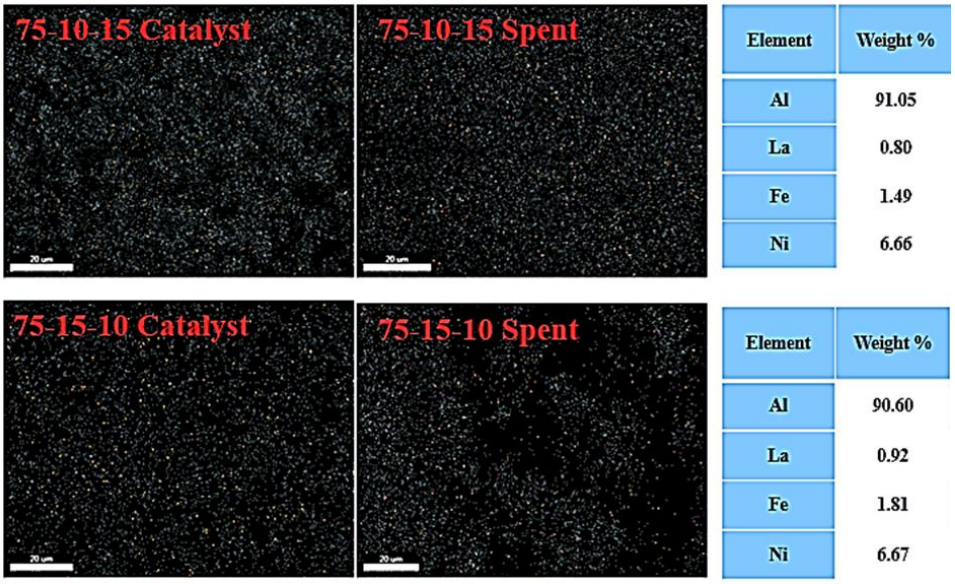

Element	Weight %
Al	91.05
La	0.80
Fe	1.49
Ni	6.66

Element	Weight %
Al	90.60
La	0.92
Fe	1.81
Ni	6.67

Fig. 5.8. EDS analysis of catalysts (a) Fresh 75Ni-10Fe-15La (b) Spent 75Ni-10Fe-15La (c) Fresh 75Ni-15Fe-10La (d) Spent 75Ni-15Fe-10La

Nickel is evenly distributed over the surface of the alumina support for both the catalysts, according to EDS elemental mapping as shown in Fig 5.8a and 5.8b. Strong peaks for Ni can be seen in the EDS spectra, indicating that it is present in considerable amounts. The Ni loading matched the theoretical values calculated during the catalyst preparation for both the catalysts. Together with nickel, iron serves as a co-catalyst and a promoter in the reforming reaction. As anticipated, the catalyst has less iron than nickel. The EDS maps reveal that iron is uniformly distributed throughout the alumina support with no signs of clustering. EDS mapping shows that lanthanum is distributed uniformly across the catalyst surface, but it is detected in smaller levels than Ni. La acts as a promoter, which increase the dispersion of Ni and Fe particles and strengthen the catalyst's ability to resist sintering. The presence of lanthanum oxide (La_2O_3) in the catalyst is confirmed by the La peaks in the EDS spectrum, which also add to its stability. Fig 5.8c and 5.8d shows that no significant change in metal dispersion is observed between fresh and spent catalysts of 75Ni-10Fe-15La and 75Ni-15Fe-10La respectively. The metal doping calculated from EDS analysis is found to be same in both fresh and spent catalysts. Further, in spent catalysts carbon is not detected during the EDS analysis which further confirms that no coke formation takes place during the reforming reaction when carried out with newly synthesize catalysts.

BET

The physisorption properties of Ni-Fe-La/Al_2O_3 catalyst is evaluated by N_2 adsorption and desorption analysis using BET curve, BJH methods. Table 5.2 represents the characteristics of trimetallic catalyst with type of isotherm.

Table 5.2 BET surface area, pore volume and pore diameter of catalysts

Catalyst	Surface Area (m^2/g)[a]	Pore Volume (cm^3/g)[b]	Pore Diameter (nm)[b]	Crystallite size (nm)c	Type of isotherm
γ Alumina	235.76	0.464	7.75	17.24	4
θ- Alumina	134	0.243	6.94	15.28	4
75Ni-20Fe-5La/Al_2O_3	114	0.168	23.36	7.17	4
75Ni-10Fe-15La/Al_2O_3	104.70	0.129	4.92	7.53	4
75Ni-15Fe-10La/Al_2O_3	107.61	0.165	6.12	7.82	4

[a] Measured by Brunauer-Emmett-Teller (BET) data.

[b] Pore volume calculated by BJH desorption method.

[c] Crystallite size of NiO calculated by Scherrer equation from XRD data

Type IV isotherm is identified for all the catalysts with hysteresis loop. Results show H1 type hysteresis loop for these catalysts identified that pore size falls in the mesopores range. Enhancement in catalytic activity is due to the better distribution of the metal within the pores and hence, surface area decreases marginally after the deposition. Higher surface area of alumina is contributing the higher active sites for the reaction. Table 5.2 represents the BET surface area of 75Ni-20Fe-5La/Al_2O_3 as 114m^2/g and pore volume 0.168m^2/g. However, large pore diameter of this catalyst, which is 23.36nm, attributed to relatively poor catalytic activity. It can be concluded that increase in metal particle size leads to poor dispersion over the surface of catalyst. Therefore, spent catalyst was also analyzed with BET analysis. The average pore size of spent catalyst increased but there is reduction in surface area and pore volume of the catalyst which could be resulted due to sintering effect for high temperature processes. There is no increase in average pore diameter of 75Ni-15Fe-10La and 75Ni-10Fe-15La conclude that no agglomeration of particles observed. The slight change in the pore diameter of 75Ni-15Fe-10La and 75Ni-10Fe-15La which shows almost same activity of the catalysts as represented. Additionally, small pores not former

into large pores during preparation of catalyst. This catalyst is calcinated at high temperature 970℃ due to which it resulted into the $LaNiO_3$ and $LaAlO_3$ phase whereas small amounts and NiO, FeO in the Ni-Fe alloy region also contribute to the gasification of carbon due to oxygen storage. The presence of these compounds can be confirmed by the XRD analysis. Moreover, carbon gasification is also promoted due to presence of La_2O_3 as shown in XRD graph in Fig 5.9.

XRD

Fig 5.9 represents XRD data of fresh and spent catalysts of 75Ni-10Fe-15La and 75Ni-15Fe-10La. There is peak at 2-theta 20° for nickel aluminate in fresh catalyst which is not present in spent catalyst XRD data. This means decomposition of nickel aluminate takes place during the hydrogen reduction process which is performed before the reaction to activate the catalyst. Simultaneously there is a peak at 52° in spent catalysts of metallic nickel. This confirm that nickel aluminate decomposes to metallic nickel during reduction process which is the cause of enhanced catalytic activity. Then peak at 2-theta 45° shows the formation of Ni-Fe alloy which attributed to the enhanced catalytic activity. This peak is present in both the catalysts and is also present in the spent catalysts. Hence, it can be concluded that the Ni-Fe alloy which was formed during the catalyst preparation and calcination was stable during the reaction and leads to enhanced catalytic activity. It should be noted that this alloy remains stable even after 130 hours of operation as shown in Fig 5.6.

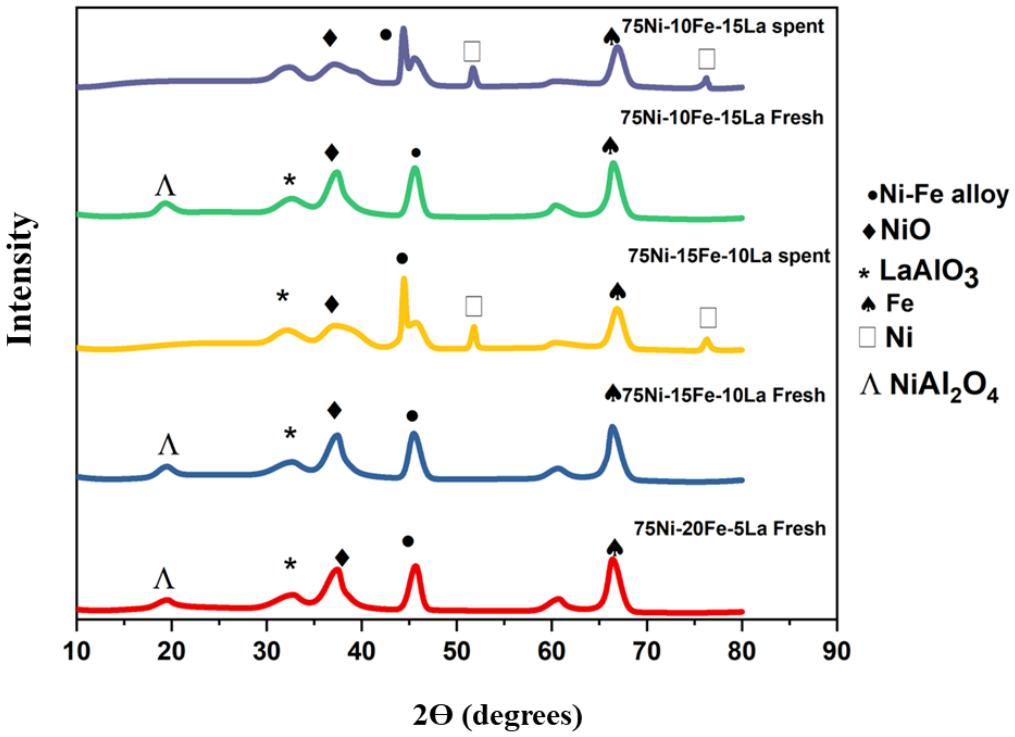

Fig. 5.9 XRD graphs of fresh and spent trimetallic catalysts

The disadvantage of nickel-based catalyst is the coke deposition which deactivates the catalyst. However, the support-metal interaction can help in reducing the coke deposition/formation. The (111), (200), and (220) planes of NiO (JCPDS 47–1049) are shown by the strong peaks in the XRD patterns at 2θ values of approximately 37.2°, 43.2°, and 62.8°. These peaks indicate that nickel is present in its oxide state (NiO), which is frequently found prior to reduction. During the reduction and steam methane reforming process, the precursor NiO changes into the active metallic Ni phase (Ni^0). Iron oxide-corresponding diffraction peaks are also seen. Peaks at around 33.2°, 35.6°, and 54.1° correspond to the hematite (Fe_3O_4) (JCPDS 33-0664) (104), (110), and (116) planes. The existence of Fe_3O_4 in the catalyst is verified by these peaks. JCPDS 19-0629 attributes (Fe_3O_4) to peaks at 30.1°, 35.5°, 43.1°, and 57.0°, in addition to hematite. The diffraction

planes for Fe_3O_4 are (220), (311), (400), and (511). During the reduction phase, Fe_3O_4 may develop and contribute to the redox cycles that stop carbon formation and depositing during the steam methane reforming process. Alumina support-specific peaks can be seen in the XRD pattern, with the (311), (222), (400), and (440) planes of θ-Al_2O_3 (JCPDS 10-0425) correlating to the principal diffraction peaks at 2θ values of 37.6°, 39.5°, 45.9°, and 66.9°. The alumina is present in a highly disordered, mesoporous phase, as indicated by the broad breadth of these peaks. This is favorable because it provides a high surface area for the dispersion of active metals (Ni, Fe, La) and leads to higher catalytic activity.

XPS

Fig 5.10 represents XPS graph of 75Ni-15Fe-10La/Al_2O_3 catalyst. The XPS graph shows the binding energy of the elements Al, Ni, Fe and La used in this catalyst. A noticeable peak in the Al 2p spectrum can be seen at 74–75 eV, which is in line with the binding energy of Al^{3+} in Al_2O_3 as represented in Fig 5.10a. The catalyst is given mechanical strength and thermal stability by the Al_2O_3 support, which also helps to disperse the active species of Ni, Fe, and La. Ni $2p_{3/2}$ and Ni $2p_{1/2}$ are the two primary peaks in the Ni 2p spectra of the Ni-Fe-La/Al_2O_3 catalyst, with binding energies that are usually between 855-857 eV and 872-875 eV, respectively as represented in Fig 5.10b. Shake-up satellite peaks provide evidence of the presence of Ni^{2+} species on the surface, indicating that Ni^{2+} is the predominant oxidation state of nickel. A lower binding energy peak about 852–853 eV also suggests the presence of Ni^{3+}, which is important for catalytic activity in SMR since metallic Ni^{3+} serves as the active phase for methane dissociation. La^{3+} is identified by distinctive peaks in the La 3d spectrum at 834–838 eV and 850–856 eV. La_2O_3, which is known to increase catalyst stability by boosting the dispersion of active metal species and preventing sintering during high-temperature reactions, is consistent with the existence of La in the +3 oxidation state as shown in Fig 5.9c.

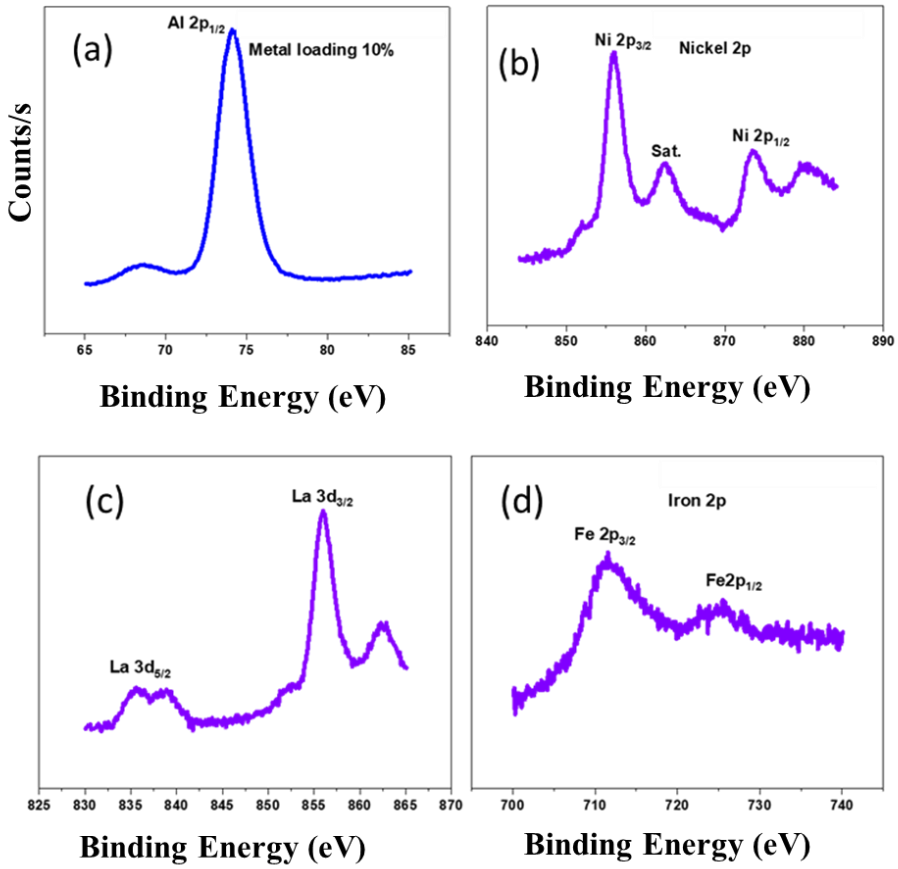

Fig. 5.10 XPS spectra Ni-Fe-La/Al_2O_3 catalyst

Therefore, this XPS result is in agreement with XRD analysis. Moreover, La_2O_3 promotes CO_2 adsorption, reducing the production of carbon during the reforming process. Fe 2p species are responsible for the peaks in the Fe 2p spectra that are seen at binding energies of roughly 710–712 eV (Fe $2p_{3/2}$) and 723–725 eV (Fe $2p_{1/2}$) as represented in Fig 5.10d. The lack of notable Fe^{3+} or Fe^{2+} peaks indicates that the majority of the surface iron is oxidized. During steam methane reforming, the Fe^{3+} species may participate in redox processes that enhance oxygen transport and inhibit carbon deposition. Strong interactions between Ni, Fe, La, and the Al_2O_3 support are suggested by the XPS data [29-33]. The synthesis of metal oxides is confirmed by the presence of Ni^{2+}, Fe^{3+}, and La^{3+} species, which may encourage synergistic effects in steam methane reforming. La seems to improve the

dispersion of Ni and Fe, reducing the likelihood of agglomeration and enhancing the stability of the catalyst at high temperatures.

FTIR

FTIR analysis performed on 75Ni-15Fe-10La and 75Ni-10Fe-15La fresh and spent catalysts is shown in Fig 5.11. Broad absorption bands in the FTIR spectrum at 3400–3700 cm^{-1} are indicative of the hydroxyl groups stretching vibrations (–OH). These peaks correspond to surface hydroxyl species that are present on the metal oxide and alumina support as a result of adsorbed water or hydroxyl groups. In the process of steam methane reforming, these surface hydroxyls are crucial for steam activation and help produce hydrogen.

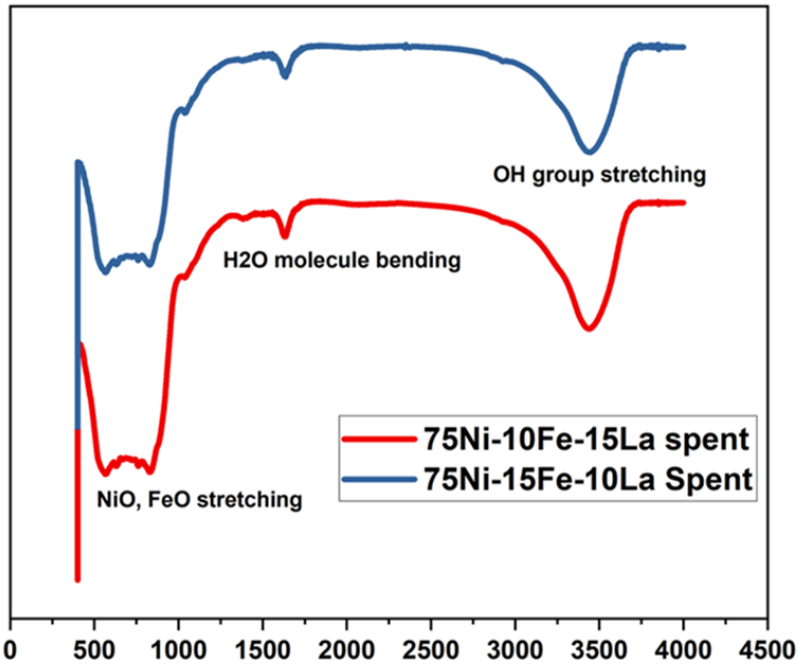

Fig. 5.11 FTIR spectra of fresh and spent 75Ni-15Fe-10La catalyst

The peak positions seen between 1400 and 1600 cm^{-1} are associated with the asymmetric stretching vibrations of surface carbonate species, or CO_3^{2-}. As a result of CO_2 adsorption

on the surface during the reforming, carbonates are present. The catalyst's lanthanum oxide (La_2O_3) is well known for its capacity to absorb CO_2 and generate surface carbonates [34]. Due to their ability to react with deposited carbon and renew active sites, these species are crucial for reducing carbon deposition, also known as coking, a prevalent problem in SMR. Ni-O and Fe-O bond stretching vibrations are responsible for the peaks in the 500–700 cm^{-1} range. These peaks existence suggests that NiO and Fe_2O_3 species are forming on the catalyst surface. These oxides are essential for the activation of methane during the reforming process. Methane dissociation's main active phase is nickel, and iron oxides may encourage redox cycles that reduces the chance of carbon deposition. The absorption bands in the 500–800 cm^{-1} range, which correspond to the Al–O stretching modes, are contributed by the Al_2O_3 support. These broad peaks overlap with those of the metal oxides, but their existence indicates that the alumina support plays a part in dispersing the active metal species (Ni, Fe, La) and offering a stable framework. Adsorbed water molecules bending vibrations are commonly detected at a wavelength of 1630–1650 cm^{-1}. This peak's existence attests to the water adsorption on the catalyst surface, which is essential for steam reforming. Through the steam reforming pathway, water molecules react with methane and surface species to produce carbon monoxide and hydrogen [35-37].

TEM

TEM analysis is done for trimetallic fresh and spent Ni-Fe-La/Al_2O_3 catalyst as shown in Fig 5.12. The support and catalyst morphology can be analyzed using TEM. The black dots on the TEM image in fresh catalyst corresponds to Fe presents in the Ni-Fe phase as shown in Fig 5.12a. The crystallite size of spent catalyst increased as compared to the crystallite size of fresh catalyst due to sintering effect for long duration. No carbon formation can be seen in both fresh and spent catalyst TEM image. Long term stability improved due to high

coke resistance which can also be seen in stability test of this trimetallic catalyst for at least 130 hours.

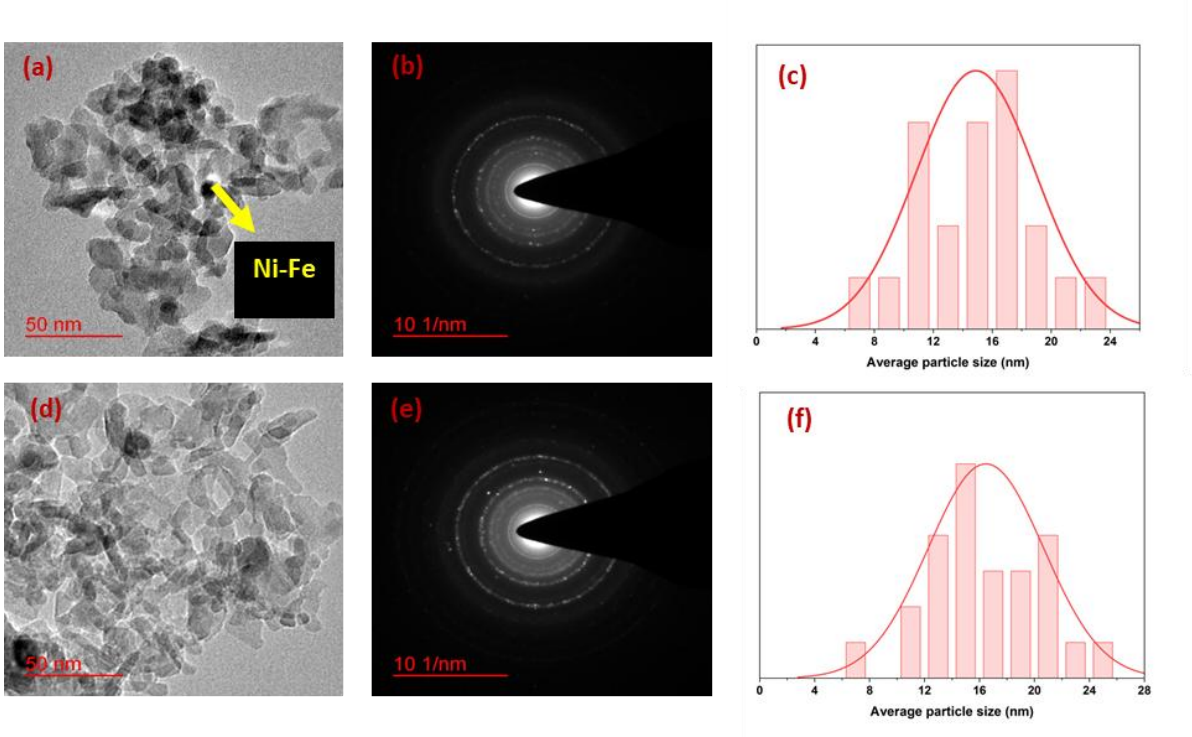

Fig. 5.12 TEM analysis of (a) Fresh 75Ni-15Fe-10La (b) SAED pattern of fresh catalyst (c) Average particle size of fresh catalyst (d) Spent 75Ni-15Fe-10La (e) SAED pattern of spent catalyst (f) Interplanar distant of spent catalyst

Spinel formation ($NiAl_2O_4$) takes place due to high temperature reaction. The Ni2+ gets deposited in the octahedral sites of alumina leads to the formation of spinel compound which can also confirmed by XRD analysis. Due to the formation of Ni spinel extent, Ni crystal size decreased. In this research, lanthanum is used as a promoter to promote the water gas shift reaction. In addition to this, the presence of La_2O_3 enhanced the metal dispersion over the surface of catalyst. Lanthanum based spinel formation also takes place with the bond between Ni and La_2O_3. The presence of La_2O_3 is also responsible of reduction in Ni crystal size. The lattice fringes shown in HRTEM pictures line up with the Ni and Fe oxide species crystallographic planes. For NiO, the measured interplanar spacings generally coincide with the (200) and (111) planes, at around 0.24 nm and 0.21 nm,

respectively. Similarly, for Fe_2O_3, the lattice fringes usually have an interplanar separation of 0.27 nm with the (104) plane. Lattice fringes that align with the (111) plane and correspond to metallic nickel (Ni^0) are detected, with an interplanar spacing of around 0.20 nm. For the steam reforming reaction to activate methane, metallic nickel must be present. La_2O_3 is characterized by the appearance of tiny crystallites scattered across the alumina support, with lattice fringes that align with the (222) planes and an interplanar spacing of around 0.29 nm. By acting as promoters, these La_2O_3 crystallites improve the stability and dispersion of Ni and Fe nanoparticles. Additionally, LaO_2 is essential for CO_2 adsorption and aids in reducing carbon deposition, or coking, during the reforming process [38-40].

5.4 Conclusions

Steam methane reforming at high temperature is investigated over trimetallic catalyst Ni-Fe-La/Al_2O_3 catalyst in packed bed reactor. The effect of promoters La and Fe is seen with Ni based catalyst. In this research, catalyst was prepared by wet impregnation method. The elemental composition was varied in the total metal loading to get the optimum values. Various characterization techniques used to analyze the catalysts. Life cycle study is also checked for atleast 130 hours. There was no deactivation of catalysts for these hours of study in terms of conversion and hydrogen yield. Carbon formation was also not taking place. Some metal sintering is observed in the spent catalyst characterization due to long time exposure of catalyst. The activity of catalyst is enhanced with the addition of promoters such as lanthanum and iron. Incorporation of lanthanum lowered the startup time of reaction. It also enhanced the dispersion of metals over the surface of catalyst. Lanthanum also used to increase the mechanical strength of catalyst. In addition to this, iron enhanced the water gas shift reaction. The presence of Ni-Fe alloy increased the catalytic activity by gasification of carbon which resulted into the formation of CO_2. The ratio of these metals is crucial in synthesizing catalysts for steam methane reforming

reaction. Moreover, the Ni-Fe alloy formation also increases the metal support interaction. High reducibility property gets enhanced with the promoted catalyst.

5.5 Cobalt based trimetallic catalyst Ni-Co-La/Al_2O_3

5.5.1 Introduction

Significant research efforts have been made to construct enhanced Ni catalysts in order to obtain catalysts with low coking and high sintering resistance [41-43]. Deposition of coke on the surface of catalyst blocks the pores which makes it challenging for long run operations by reducing the catalyst activity. Industrially, coke deposition is avoided using high stoichiometric ratio of steam/methane but this can lead to high pressure drop. Therefore, in the literature cobalt has emerged as an active metal catalyst for C-C bond scission, which is an important characteristic for steam methane reforming. Many researchers reported cobalt in reducing the coke formation of the catalyst [44-46]. Cobalt facilitates the gasification of coke deposition which leads to oxidation of carbonaceous species to CO_2 by preventing accumulation of carbon over surface of catalyst. In addition to this, the choice of support strongly affects the cobalt dispersion, particle size and reducibility, thereby altering the catalytic activity. Many metal oxide materials have been used as catalyst supports for cobalt including Al_2O_3, ZrO_2, SiO_2, CeO_2 and ZnO [47-52]. Ishihara et al., also reported higher catalytic activity of Co supported on alumina as compared to Zirconia [53]. An extensive study has been dedicated in recent years to modifying the characteristics of nickel and cobalt catalysts to improve their performance and stability in SMR applications.

Furthermore, efforts have been undertaken to investigate novel promoters and additives that reduce deactivation and improve catalytic viability over time. These catalysts promote the dissociation of methane and water vapor, make carbonaceous species removal easier via water-gas shift reactions, and reduce the formation of unwanted byproducts. In

literature, lanthanum was reported to promote the water gas shift reaction and getting maximum conversion at low temperature [54]. Lanthanum oxide possesses high oxygen mobility. It will facilitate the adsorption of steam molecules on the surface of catalyst. Moreover, iron was also reported to enhance the water gas shift reaction by lowering the CO selectivity [55]. Iron oxide also possesses high oxygen storage properties by providing redox reactions. Therefore, in this paper, a series of studies performed focusing on trimetallic catalyst for steam methane reforming on alumina and ceria supports. Iron and lanthanum were used as promoters to promote the water gas shift reaction. Therefore, Ni-Co combination was tested with the addition of lanthanum as promoter by varying the Co-La ratio. Similarly, Ni-Co combination was tested with the addition of iron as promoter by varying the Co-Fe ratio. And, the effect of Ni based trimetallic catalyst on both the supports Al_2O_3 and CeO_2 supports was studied for steam methane reforming. The performance of the catalyst is dependent on nature of the supports, active metal combination, particle size. This includes investigations of catalytic activity and stability of cobalt based catalysts. Some of the characterization techniques implemented in these studies involve XRD, SEM, EDS, BET, FTIR, TEM. A series of optimization studies has been investigated the influence of independent variables such as reaction temperature, W/F, Steam to water ratio, and life cycle analysis.

Table 5.3 Literature survey

Catalyst	Reaction conditions	Remarks	Authors
Ni-Co bimetallic catalyst supported on hollow sphere Al_2O_3	700°C, 1 atm, CH_4:H_2O = 1:3	Hollow sphere Al_2O_3 support improves dispersion of Ni-Co particles, enhancing activity and stability.	Jelyani et al., 2022 [56]
Ni-Co bimetallic catalyst supported on Al_2O_3 nanostructures	400–550°C, 1 atm, CO_2:H_2 = 1:4	Promoters improve CO_2 adsorption and H_2 dissociation, achieving high CO_2 conversion and CH_4 selectivity.	Shafee et al., 2021 [57]
Ni-Co/Al_2O_3 bimetallic catalyst	800°C, 1 atm, CH_4:H_2O = 1:3	Co enhances coke resistance by improving carbon gasification and reducing metal particle sintering.	You et al., 2014 [10]
Ni-Co/Al_2O_3 bimetallic catalyst	650°C, 1 atm, C_2H_5OH:H_2O = 1:3	Ni-Co catalysts improve hydrogen production from ethanol steam reforming, with increased stability and activity.	Romero et al., 2022 [58]
Ni-Co/$MgAl_2O_4$	Separate CH_4 decomposition and CO_2 activation	Focused on syngas production with minimal carbon deposition and good stability	Deng et al., 2025 [59]
Co/γ-Al_2O_3,Fe/γ-Al_2O_3	Catalytic methane pyrolysis	CO_2-free hydrogen production using Co-based and Fe-based catalysts	Pachatouridou et al., 2025 [60]

Cobalt and Nickel-based Nanomaterials	Catalytic reforming of hydrocarbons and oxygenates to hydrogen-rich syngas	Focuses on synthesis and application of Co and Ni-based nanomaterials for reforming hydrocarbons	Mageed et al., 2024 [61]
Ni-Co-La/Al_2O_3 (Current work)	500-800°C, 1atm, S/M 4:1	Suppressed carbon formation results in zero CO selectivity with maximum conversion at 500°C	

The literature on Ni-Co/Al_2O_3 catalysts for steam methane reforming highlights significant advancements in catalyst design, activity, and stability. Jelyani et al. [56] demonstrated the effectiveness of Ni-Co bimetallic catalysts supported on hollow sphere Al_2O_3, where the unique support structure improved the dispersion of Ni-Co particles, leading to enhanced catalytic activity and stability at high temperatures. Shafee et al. [57] further advanced this concept by using promoted Ni-Co/Al_2O_3 nanostructures, achieving improved CO_2 adsorption and hydrogen dissociation, which increased CO_2 conversion and CH_4 selectivity during reforming reactions. In a different study, You et al. [10] focused on Ni-Co/Al_2O_3 catalysts and identified cobalt's role in enhancing coke resistance, which was critical for maintaining long-term catalyst stability by preventing carbon deposition and metal sintering at high temperatures. Lastly, Romero et al. [58] explored the use of Ni-Co/Al_2O_3 bimetallic catalysts for ethanol steam reforming, where the catalysts showed promising hydrogen production performance with excellent stability, making them suitable for industrial applications in renewable hydrogen production. These studies collectively underscore the importance of catalyst composition and support structure in improving the performance of Ni-Co/Al_2O_3 catalysts for various reforming reactions.

5.5.2 Methodology

Catalyst Preparation

Monometallic, bimetallic and trimetallic catalysts supported on alumina and ceria were prepared by wet impregnation method. To synthesize Ni-Co/Al_2O_3 catalyst, commercially available Al_2O_3 (Sigma-Aldrich) was impregnated with Ni and Co using precursor solutions of $Ni(NO_3)_2 \cdot 6H_2O$ (98% purity, SRL chemicals) and $Co(NO_3)_2 \cdot 6H_2O$ (98% purity, SRL chemicals) with Ni/Co ratio of 3/1 with a total metal loading of 10% [62]. Similarly, Ni-Co/CeO_2 was synthesized with the impregnation of Ni and Co on CeO_2 (Supplied from Himedia) as support with total metal loading of 10%. Afterwards, a trimetallic catalyst Ni-Co-La/Al_2O_3 was prepared with precursor solution of Ni $(NO_3)_2 \cdot 6H_2O$, Co $(NO_3)_2 \cdot 6H_2O$, and La $(NO_3)_2 \cdot 6H_2O$ having Ni/Co/La scale of 75/20/5 with total metal loading of 10%. Similarly, trimetallic Ni-Co-Fe (precursor solution Ni $(NO_3)_2 \cdot 6H_2O$, Co $(NO_3)_2 \cdot 6H_2O$, and Fe $(NO_3)_2 \cdot 9H_2O$) was also prepared to compare the results with Ni-Co-La with the same Ni/Co/Fe scale of 75/20/5.

Then solution as per the requirement based on catalyst was left for vigorous stirring for at least 4 hours for nucleation growth. Thereafter, this solution was slowly evaporated at temperature 70℃. The final slurry was dried in the vacuum for overnight. Finally, the samples were calcined at a temperature of 970℃ with a heating rate of 1℃/min. After calcination, the catalyst was palletized and crushed using mortar pestle and finally sieved to 180-300 microns size which was used for catalyst testing in packed bed reactor.

5.5.3 Catalyst characterization

X-ray Diffraction (XRD) patterns were obtained with a (Rigaku XRD analyzer) in the 2θ range of 0-90℃ using Cu-kα radiation operated at 20 kV. XRD confirmed the crystallinity phase of catalysts by obtaining sharp peaks. The crystal size of catalysts was calculated by Scherrer equation (Eq. 5.1) with the data obtained by XRD analysis. The

experimental error involved in angle measurement was ± 0.02°C. The peaks angles were identified by comparing the XRD data of catalysts with the literature reported values using X-Pert software.

$$k\lambda = d\,\beta\cos\theta \quad (5.1)$$

Where d is the crystallite size, k is the constant (for spherical particles, k value is 0.94), λ is the X-ray wavelength which is 1.54 Å for Cu-kα radiation. β is the FWHM (Full width half maxima) measured in radians and θ is angle of diffraction.

The specific surface area was measured by BET (Braunauer Emmett Teller) via nitrogen adsorption desorption at -196°C and pore volume, average pore diameter was measured by BJH (Barret-Joyner-Halenda) desorption method using BET instrument (Meso 112®). All the samples were initially degassed at 250°C for 2 hours in vacuum. After degassing, the samples were analyzed for adsorption-desorption isotherm.

The surface morphology, metal dispersion and microstructures were examined by Scanning electron microscope (SEM) analysis (Nova Nano SEM 450). Different SEM images were recorded at various magnifications and resolution upto 5 microns. Elemental mapping was performed by using EDS analysis (EDAX Inc.).

Transmission electron microscope (TEM) was carried out on fresh and spent catalyst in high resolution Tecnai G2 20 TWIN instrument. Prior to TEM analysis, samples were prepared by sonication of catalysts in ethanol for 1 hour. After preparing sample, one drop of solution was dispersed on the carbon coated TEM grid. Then the TEM grid was kept for drying for overnight.

FTIR (Fourier transform infrared spectroscopy) spectra of fresh and spent catalyst were observed using THERMO Electron scientific instruments LLC. The graph of transmittance vs wavelength was obtained using FTIR analysis. Various functional groups on the catalyst surface were identified by analyzing the adsorption band in the spectrum.

5.5.4 Catalyst testing

Steam methane reforming tests were performed at atmospheric pressure in a packed bed reactor where the catalyst is filled at the bottom section of the reactor. The Inconel reactor with an internal diameter of 11.74mm was thermally insulated to avoid any heat loss to the reactor. The temperature of catalyst bed was monitored using K-type thermocouple mounted on the top of the catalyst bed. The schematic diagram of catalytic reformer is shown in Fig 5.13. The Catalyst (180-300 microns) weighed 0.76gm mixed with quartz in 1:1 ratio was placed at the middle section of the reactor where temperature was uniformly maintained. Initially, the catalyst was reduced in the presence of 10 vol% H_2 in nitrogen gas environment for 4 hours at 900 ℃. The temperature of the reaction was varied from 500-800℃.The experiments were performed at S/M 1:4, W/F 26.8 kg_{cat}. s/mol. Water was fed to the packed bed reactor using high pressure metering pump (Eldex optos pump, USA) and gases flow were maintained through mass flow controllers (Bronkhorst).

The mixture of CH_4, N_2 and steam was preheated up to the reaction temperature. The outlet of the reactor was connected to the condenser to condensate excess of water and then condensate was collected and separated using gas liquid separator. The reactor effluent consists of H_2, CO, CO_2, unreacted CH_4 were analyzed using gas chromatography (Nucon GC 1105 trace). The gases were analyzed using a thermal conductivity detector (TCD) using Porapaq Q (I.D 2mm, length 1m) and Molecular sieve column (I.D 2mm, length 3m) arranged in parallel. The conversion (Eq. 5.2), CO_2 selectivity (Eq. 5.3), CO selectivity (Eq. 5.4), and H_2 Yield (Eq. 5.5) was calculated by using GC data.

$$\%X_{CH_4} = \left(\frac{f_{CO,out} + f_{CO_2,out}}{f_{CH_4,out} + f_{CO,out} + f_{CO_2,out}}\right) * 100 \quad (5.2)$$

$$\%S_{CO_2} = \frac{f_{CO_2,out}}{f_{CO,out} + f_{CO_2,out}} * 100 \quad (5.3)$$

$$\%S_{CO} = \frac{f_{CO,out}}{f_{CO,out} + f_{CO_2,out}} * 100 \quad (5.4)$$

$$Y_{H_2} = \frac{(f_{H_2})out}{(f_{CH_4})in} \quad (5.5)$$

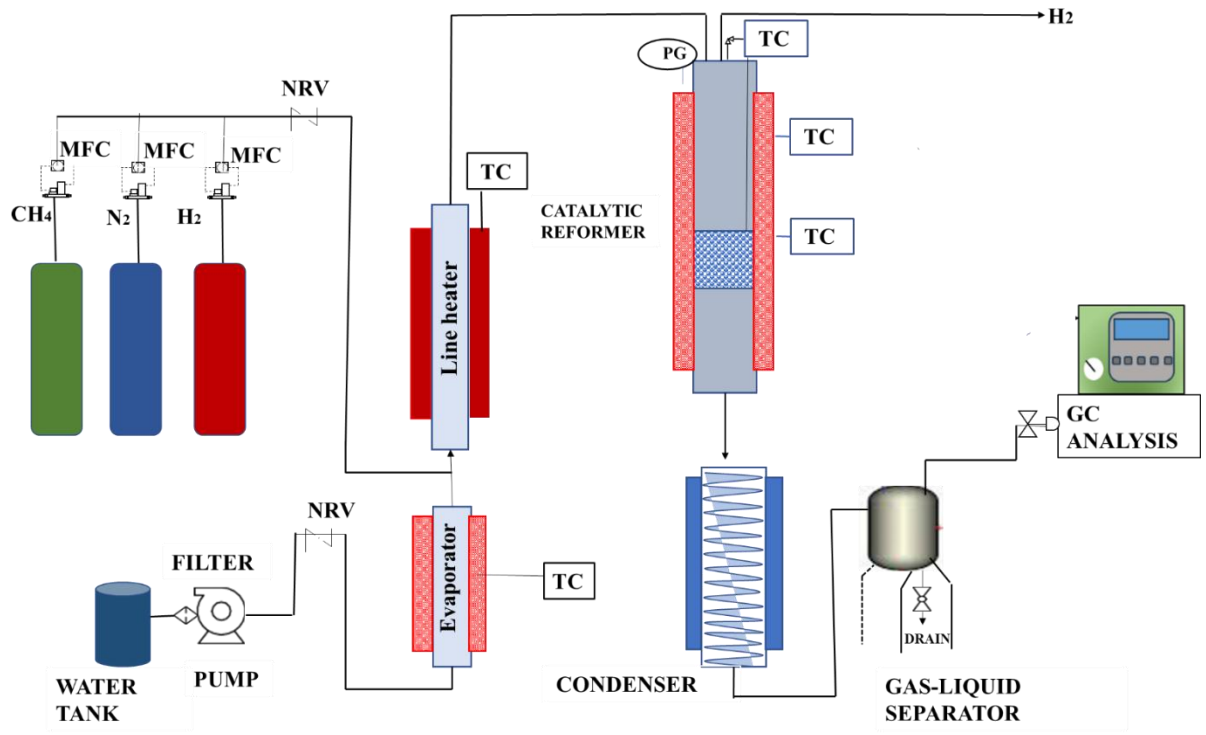

Fig. 5.13 Schematic diagram of catalytic reformer

Results and discussion

5.6.1 Characterization results

XRD

Fig 5.14 represents the XRD graph of all the catalysts supported on alumina and ceria supports. Monometallic, bimetallic and trimetallic catalysts of Ni, Co combinations are characterized by XRD. The diffraction angles, phases crystallinity of all the catalysts are identified by this technique. The peak identified for Co/CeO_2, La/CeO_2, $Co\text{-}La/CeO_2$ and $Ni\text{-}Co/CeO_2$ at 2Θ Values of 28.560, 33.096, 47.506, 56.370, 59.119, 69.451, 76.742,79.119, 88.480 with the diffraction planes for ceria supported catalysts are (1 1 1), (0 0 2), (0 2 2), (1 1 3), (2 2 2), (0 0 4), (1 3 3), (0 2 4), (2 2 4). The ceria supported catalysts

having lattice constant of 5.409 Å (JCPDS reference no 98-008-6411). It is for cubic crystal system with a space group of Fm-3m (ICSD Collection code 621710). While for alumina supported catalysts, the peak values centered at 2Θ values 39.482, 45.912, 66.951, 80.599, 84.993 for diffraction planes (1 1 1), (0 2 2), (1 1 3), (2 2 2) . All the alumina supported catalysts having lattice constant of 2.86Å (JCPDS reference no 98-001-3120). It is also of cubic crystal system with space group of Fm-3m (ICSD Collection code 30267). The crystallite size of La/CeO_2, Co/CeO_2, Ni-Co/CeO_2, Co-La/CeO_2 supported catalysts are calculated by Scherer's equation is 25.45nm for 2Θ value of 28.45, 64.07nm for 2θ value of 28.57, 51.16nm for 28.60 and 42.24nm for 28.55 respectively. Similarly, crystallite size of La/Al_2O_3, Co/Al_2O_3, Ni-Co/Al_2O_3, Co-La/Al_2O_3, Ni-Co-La/Al_2O_3, Ni-Co-Fe/Al_2O_3, and spent Ni-Co-La/Al_2O_3 calculated by Scherer's equation is 10.12, 9.15, 7.33, 7.48, 6.68, 9.46, and 7.58nm respectively.

The NiO peak is observed in both Ni-Co/CeO_2 and Ni-Co/Al_2O_3 catalysts with different intensities and shift in 2Θ angle which also indicates various crystal sizes. The peak assigned to 43.73° is present in all the catalysts which attributed to NiO phase. The successful incorporation of metallic nickel into the catalysts is confirmed by the existence of Ni peaks. [64] Ni peaks with greater intensity indicate superior crystallinity, which may affect catalytic activity. Some peaks correspond to NiO, which indicates that Ni in the precursor catalyst exists in an oxidized form. NiO is usually reduced to metallic Ni during catalyst activation before the methane reforming reaction takes place. Characteristic peaks of Al_2O_3 are visible in the XRD patterns of catalysts containing this oxide, which aid in stabilizing Ni particles and avoiding sintering during high-temperature reactions. [63]

The peak at 37.23 and 31.23° is assigned to Co species Co_2O_3 and Co_3O_4 in cobalt catalysts respectively. Co_2O_3 peak observed in ceria supported catalysts and Co_3O_4 peak observed in alumina supported catalysts. The diffraction peaks corresponding to cobalt oxides

confirm their presence in certain catalysts. Cobalt-based catalysts are known for their high catalytic activity, particularly in enhancing the dispersion of Ni and improving resistance to carbon deposition.[65]

In trimetallic Ni-Co-Fe/Al_2O_3 catalyst, Ni-Fe alloy peak is observed at 45.23.

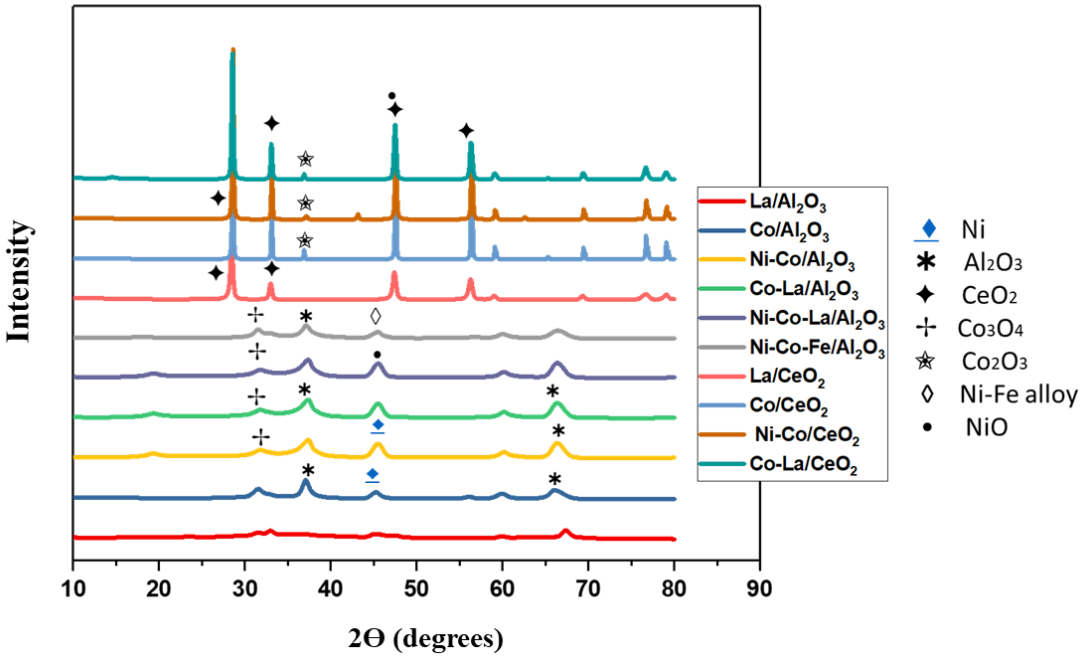

Fig. 5.14 XRD graph of alumina and ceria supported catalysts

Strong metal contacts are suggested by the presence of a Ni-Fe alloy (◇), which enhances catalytic activity and decreases sintering. Fe also alters the electronic structure of Ni, which lessens the tendency for coke production. Similar diffraction peaks for Ni, Co oxides, and AlO_3 are seen in the Ni-Co-La/Al_2O_3 catalyst. The inclusion of La improves oxygen mobility, stabilizing the active metal sites and boosting coke resistance. Peaks for CeO_2 (*) are seen on the Ni-Co-La/CeO_2 catalyst supported on ceria, indicating its function in oxidizing deposited carbon and storing oxygen through redox processes. In this system, the metal-support interactions improve the catalytic lifespan and activity. All things considered, trimetallic catalysts have a number of benefits over monometallic and bimetallic systems, such as better metal synergy, increased resistance to coke formation,

improved reducibility because of the interaction between Ni, Co, and Fe or La, and enhanced thermal stability. These active phases, which are essential for maximizing the durability and efficiency of steam methane reforming, are confirmed to have formed by the XRD examination. As the nitrate species leave the cobalt surface, formation of Co_3O_4 is observed in a cubic phase. Regarding the XRD pattern, the formation of crystalline Co_3O_4 is only observable above 250°C. The largest crystallite size of Co is observed in Co/CeO_2 which is 64.07nm which can be attributed to the poor catalytic activity of the catalyst. Whereas, in Ni-Co combination, largest crystal size is observed in $Ni\text{-}Co/CeO_2$ as compared to all alumina supported catalyst which can also be responsible for the lower catalytic activity of ceria supported catalyst over alumina. [66]

Different phases, including Ni-Co alloys, metal oxides, and support materials, are represented as peaks in the diffraction pattern. These phases affect the stability and reactivity of the catalyst. While La-based oxides help with thermal stability and resistance to carbon deposition, CeO_2 enhances oxygen storage and redox characteristics.

BET

Fig 5.15(a) and (b) show BET adsorption and desorption isotherms of all the ceria supported and alumina supported catalysts respectively. Table 5.4 represents the surface area, pore volume, pore diameter and crystal size of all the catalysts. The pore size of all the catalysts falls in the range of mesoporous that lies between 2-50nm. The BET table highlights variations in surface area, pore volume, pore diameter, crystallite size, and isotherm type, offering important insights into the textural characteristics of different catalysts employed in steam methane reforming. Because of its mesoporous character, as demonstrated by its Type IV isotherm, $\gamma\text{-}Al_2O_3$ is the catalyst with the biggest surface area (235.76 m^2/g) and pore volume (0.464 cm^3/g), making it the perfect support for metal dispersion. CeO_2 and its derivatives, on the other hand, have much smaller pore volumes

and surface areas (5.4 to 19.2 m^2/g), indicating that CeO_2-based catalysts have a denser, less porous structure that might influence gas diffusion and active site availability as discussed in previous chapter.

Table 5.4 BET analysis of all the catalysts

Catalyst	Surface Area (m^2/g)	Pore Volume (cm^3/g)	Pore Diameter (nm)	Crystal Size (nm)	Type of isotherm
Ni-Co/ Al_2O_3	95.31	0.167	26.56	7.33	4
Ni-Co-Fe/ Al_2O_3	64.34	0.107	29.46	9.46	4
Ni-Co-La/ Al_2O_3	83.44	0.143	22.31	6.68	4
Spent Ni-Co-La/ Al_2O_3	77.02	0.105	19.7	7.58	4
Spent Ni-Co-Fe/ Al_2O_3	55.34	0.086	20.45	9.74	4

[a] Measured by Brunauer-Emmett-Teller (BET) data.

[b] Pore volume calculated by BJH desorption method.

[c] Crystallite size of NiO calculated by Scherrer equation obtained from XRD analysis

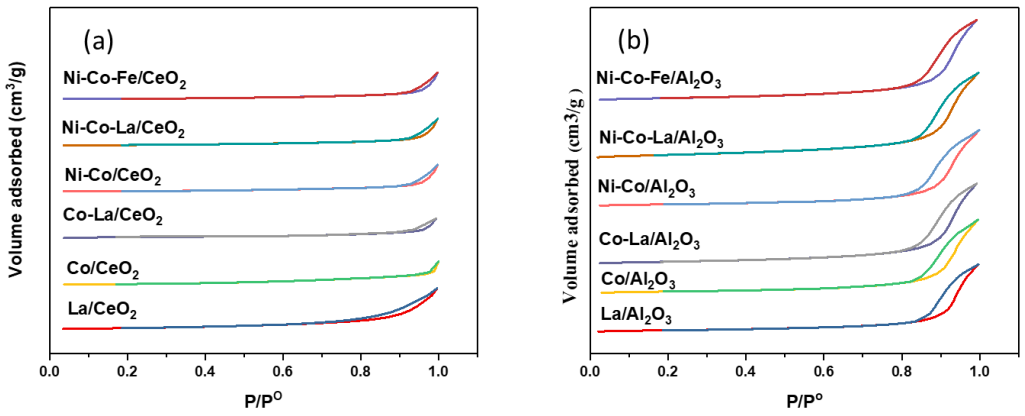

Fig. 5.15 Adsorption-desorption isotherm of (a) ceria supported (b) alumina supported catalysts

These textural characteristics are changed when Ni, Co, and La are added to Al_2O_3. Ni/Al_2O_3 retains a moderate crystallite size (13.375 nm) and a moderately high surface area (106 m^2/g), both of which are advantageous for catalytic activity. Likewise, trimetallic and

bimetallic catalysts, including Ni-Co-La/Al_2O_3 and Ni-Co-Fe/Al_2O_3, exhibit mesoporous structures with moderate surface areas, promoting improved metal dispersion and gas transport. Alumina-based catalysts usually have smaller pore diameters (6–29 nm), which enable effective methane reforming. In contrast, CeO_2-based catalysts have larger pore diameters (up to 37.12 nm in Ni-Co/CeO_2), which may affect metal-support interactions. Pore diameter variations also affect catalyst behavior. The isotherm categorization also demonstrates that CeO_2-based catalysts typically display Type III isotherms, indicating a lower degree of porosity, whereas alumina-based catalysts primarily follow Type IV isotherms, indicating mesoporosity. Long-term catalytic stability is adversely affected by spent catalysts, such as Spent Ni-Co-La/Al_2O_3 and Spent Ni-Co-Fe/Al_2O_3, which exhibit decreased surface area and pore volume, most likely as a result of sintering or coke deposition. The difficulties with catalyst deactivation are brought to light by this degradation, underscoring the necessity of regeneration techniques or better formulations to increase performance and durability. All things considered, the BET analysis emphasizes how important support materials, metal additives, and structural characteristics are to maximizing catalyst performance for steam methane reforming, where stable and effective catalytic behavior is facilitated by high surface area, balanced porosity, and regulated crystallite size.

The degree of metal dispersion and possible sintering effects are indicated by the crystallite size, which is determined using the Scherrer equation from XRD measurements. While bigger crystallites can cause metal agglomeration, which lowers the available surface area for reactions, smaller crystallite sizes often increase catalytic activity by increasing the number of exposed active sites. While γ-Al_2O_3 and θ-Al_2O_3 have significantly higher crystallite sizes of 17.24 nm and 15.28 nm, respectively, which nevertheless lie within a range that allows effective catalytic performance, Ni/Al_2O_3 has a relatively tiny crystallite

size of 13.375 nm, suggesting adequate metal dispersion. The crystallite sizes of CeO_2-based catalysts, including Ni/CeO_2 and La/CeO_2, are noticeably bigger (24.54 nm and 25.45 nm, respectively), which may reduce catalytic efficiency because of the reduced exposure of the active surface. Co/CeO_2 and Co-La/CeO_2 stand out in particular because of their extraordinarily large crystallite diameters, measuring 64.07 nm and 42.24 nm, respectively, which signify severe particle agglomeration and decreased metal dispersion. Because there are fewer active Ni or Co sites accessible for methane reforming reactions, these bigger crystallites may have a detrimental effect on catalytic activity.

Different crystallite sizes in bimetallic and trimetallic catalysts, as Ni-Co/CeO_2 (51.16 nm) and Ni-Co-Fe/Al_2O_3 (9.46 nm), indicate various levels of metal interaction and dispersion. With a crystallite size of 6.68 nm, Ni-Co-La/Al_2O_3 exhibits good dispersion, which can maximize metal-support interactions and lead to increased catalytic activity. The crystallite size of the spent catalysts, especially Spent Ni-Co-La/Al_2O_3 and Spent Ni-Co-Fe/Al_2O_3, increases from 6.68 nm to 7.58 nm and from 9.46 nm to 9.74 nm, respectively, in comparison to their fresh counterparts. This suggests sintering and particle growth over time. The influence of thermal sintering during long-term steam methane reforming is further supported by this rise in crystallite size, which is correlated with the observed decrease in surface area and pore volume.

SEM/EDS

Fig 5.16a-k represents the SEM images of ceria and alumina supported catalysts. The surface morphology of various catalysts used in steam methane reforming (SMR), such as bimetallic and trimetallic compositions supported on CeO_2 and Al_2O_3, can be understood from the SEM images. Different catalysts are depicted in Fig. 5.16 (a–h), which display variations in particle size and metal dispersion. There are notable morphological differences between the trimetallic catalysts Ni-Co-La/Al_2O_3 (image i) and Ni-Co-Fe/Al_2O_3

(image j). The surface of the Ni-Co-La/Al_2O_3 catalyst is finely structured and widely distributed, which is essential for enhancing catalytic stability and activity. Lanthanum (La) is a crucial component in improving metal dispersion, inhibiting sintering, and decreasing coke deposition all of which are necessary for long-term SMR applications.

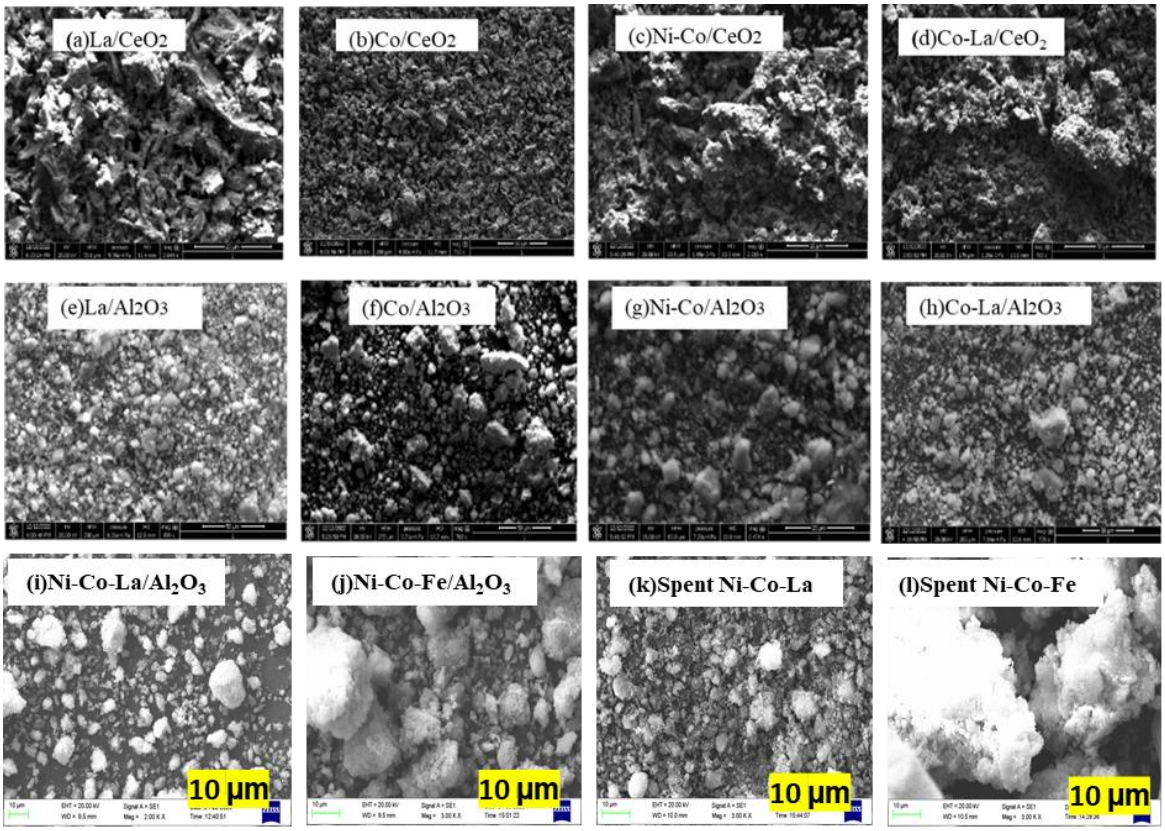

Fig. 5.16 SEM images of a) La/CeO_2, b) Co/CeO_2, c) Ni-Co/CeO_2, d) Co-La/CeO_2, e) La/Al_2O_3, f) Co/Al_2O_3, g) Ni-Co/Al_2O_3, h) Co-La/Al_2O_3 (i) Ni-Co-La/Al_2O_3 (j) Ni-Co-Fe/Al_2O_3 (k) Spent Ni-Co-La/Al_2O_3 (l) Spent Ni-Co-Fe/Al_2O_3

The larger metal particles in Ni-Co-Fe/Al_2O_3, on the other hand, could result in more sintering, which would impair its catalytic effectiveness over time. The distinctions in durability between these two trimetallic compositions are further demonstrated by the spent catalysts (k, l). Superior thermal stability and resistance to deactivation are confirmed by the spent Ni-Co-La/Al_2O_3 catalyst ability to maintain a comparatively stable structure with little aggregation. Nevertheless, following extended usage, the spent Ni-Co-Fe/Al_2O_3 catalyst shows considerable particle aggregation and potential sintering, suggesting

decreased efficiency. Because of its superior resistance to deactivation, high catalytic efficiency, and long-term stability under reaction circumstances, these data validate that Ni-Co-La/Al_2O_3 is the best-performing catalyst for SMR. For industrial methane reforming applications, where catalyst efficiency and durability are crucial, this makes it an excellent choice. [67-69]

The crystal size of Ni-Co/Al_2O_3 was smaller than Co/Al_2O_3 which is attributed to the good dispersion of metal over the surface of support by avoiding the agglomeration of particles which can be seen in Fig 5.16 (f), (g) [70]. Nevertheless, the pore volume of Ni-Co/Al_2O_3 decreased after the addition of cobalt, which is attributed to the porous doping in the Ni-Co combination. Moreover, the alumina-supported catalysts having high surface area and pore volume than ceria supported catalysts. This property also contributes to be one of the reasons for increased catalytic activity of catalysts supported on alumina. It can be seen from Fig 5.16 (a), (b), (c), and (d) that there is poor dispersion of metals over the surface of the support. cluster formation can also be seen in the images. Compared to ceria-supported images, metal on alumina-supported catalysts is having good dispersion. But support can be seen in big pieces. Among all the alumina supported catalysts, Ni-Co/Al_2O_3 catalyst is having better dispersion which can also responsible for the good catalytic activity. Therefore, Ni-Co/Al_2O_3 has chosen for the further study in this research with effect of promoters. For trimetallic catalyst, Ni-Co-La/Al_2O_3 metals are well dispersed on the surface of catalyst. No carbon nanotube formation was observed on the surface of spent catalyst of Ni-Co-La/Al_2O_3 after long run for 130 hours. But bigger particles can be clearly observed in the Ni-Co-Fe/Al_2O_3 catalyst in the SEM image. Therefore, it can be confirmed that less traces of carbon formation takes place in spent lanthanum based trimetallic catalyst after long run.

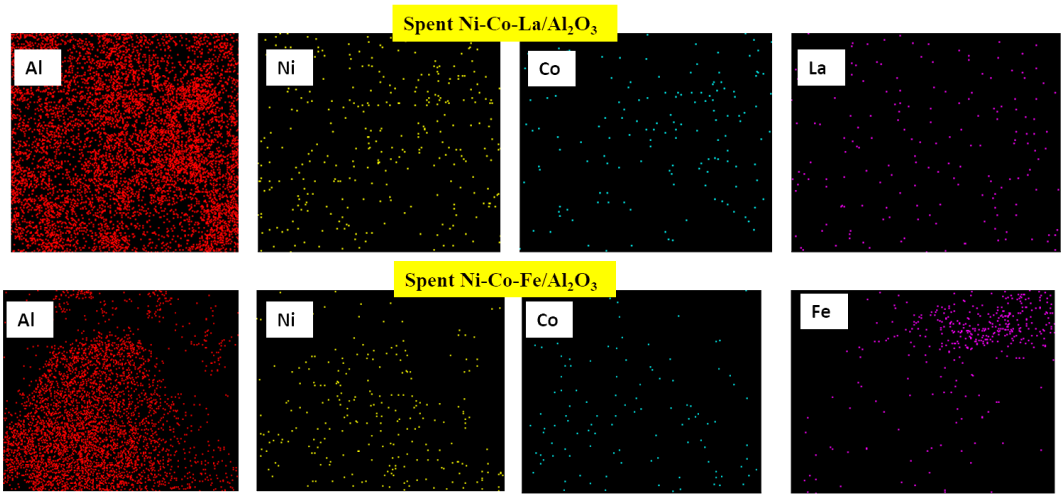

Fig. 5.17 EDS images (a) Spent Ni-Co-La/Al_2O_3 and d) Spent Ni-Co-Fe/ Al_2O_3

Elemental composition of all the catalysts were confirmed by the EDS analysis as represented in Fig 5.17. It was observed from EDS images that metals are well dispersed on the surface of Ni-Co-La/Al_2O_3 catalyst. All the elements such as Ni, Co, Fe and La is evident from the EDS analysis. The elements were confirmed with amounts as calculated during synthesis process of catalyst. There is no carbon formation observed in both trimetallic catalysts.

TEM

The morphology, crystallinity, and particle size distribution of various catalysts employed in steam methane reforming (SMR) are all significantly revealed by the Transmission Electron Microscopy (TEM) results. TEM micrographs, particle size distribution graphs, and Selected Area Electron Diffraction (SAED) patterns are the three main categories into which the images are divided.

The nanoscale shape of the catalysts is seen in the TEM pictures (leftmost column). These pictures show how the metal nanoparticles are distributed on the support, emphasizing their surface coverage, agglomeration patterns, and form. Because they have a larger active surface area, smaller and well-dispersed nanoparticles show superior catalytic activity and

stability. The Ni-Co-La/Al_2O_3 catalyst exhibits the best and most consistent dispersion of nanoparticles among the other catalysts. La improves the stability of Ni and Co nanoparticles by limiting excessive agglomeration and preserving a smaller particle size, both of which are essential for long-term catalytic activity.

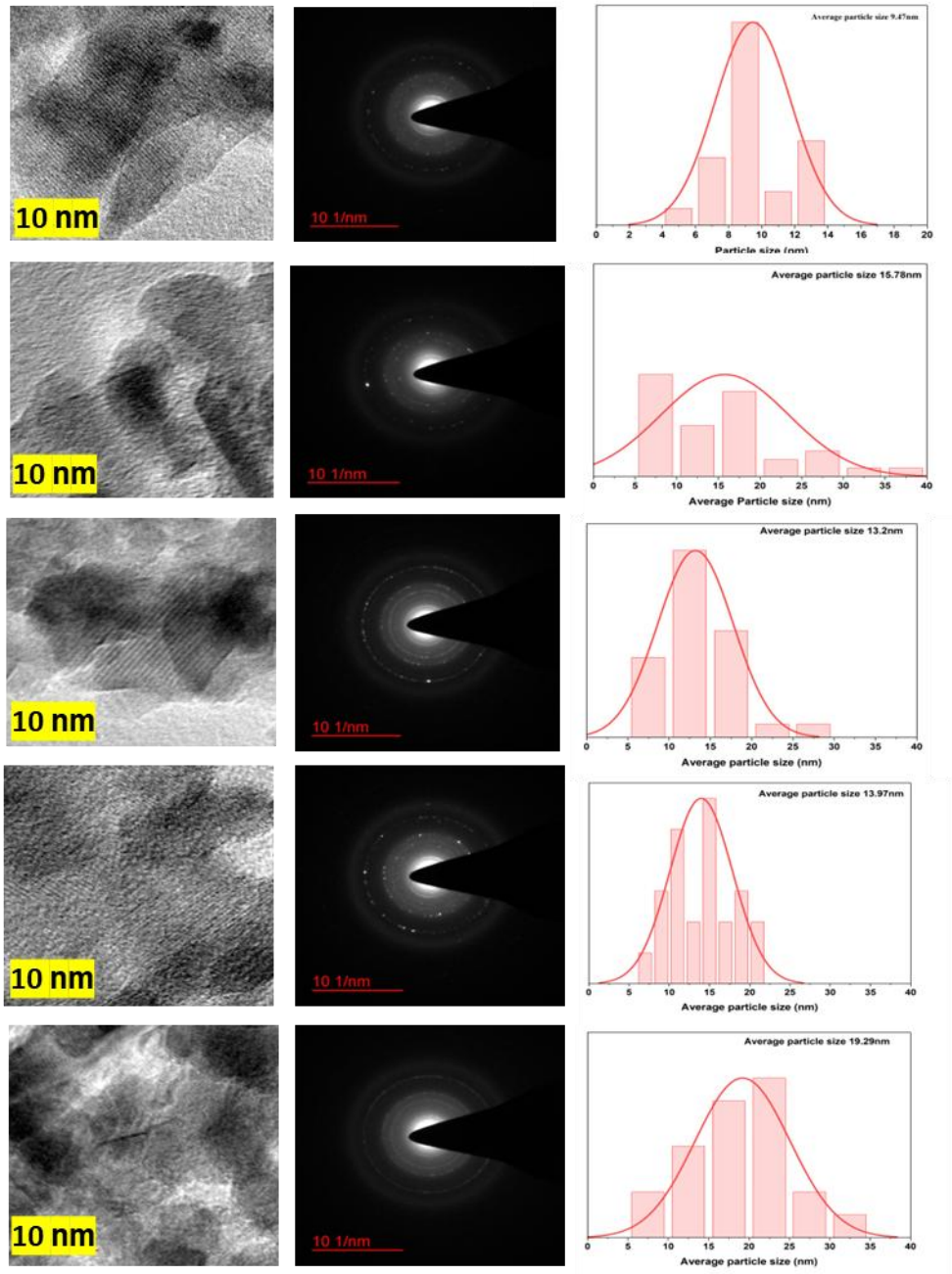

Fig. 5.18 TEM images of a) Ni-Co/Al_2O_3, b) Ni-Co-Fe/Al_2O_3, c) Ni-Co-La/Al_2O_3 d) Spent Ni-Co- La/Al_2O_3 and e) Spent Ni-Co- Fe/Al_2O_3

The crystalline nature of the catalysts is revealed by the Selected Area Electron Diffraction (SAED) pictures (middle column). A polycrystalline structure is shown by the circular diffraction rings, which match the distinctive planes of the metallic phases and support materials. Sharp, distinct rings on the Ni-Co-La/Al_2O_3 catalyst attest to its extremely crystalline character. Because it helps sustain active metal sites over prolonged reaction times, this crystallinity improves catalyst endurance. On the other hand, catalysts with diffuse or wider diffraction patterns can contain more amorphous material, which could result in less stability during the reaction. The distribution of metal nanoparticles in each catalyst sample is seen in the particle size analysis graphs (rightmost column). Different catalysts have typical particle sizes ranging from about 9.47 nm to 19.29 nm. Since they increase the catalyst active surface area, increase hydrogen output, and decrease carbon deposition, smaller particle sizes are typically favored for SMR. With an ideal particle size of around 9.47 nm to 13.97 nm, the Ni-Co-La/Al_2O_3 catalyst exhibits a very narrow size distribution, suggesting better metal dispersion and well-controlled synthesis. On the other hand, catalysts with bigger particle sizes (like 19.29 nm) might have decreased activity over time because of increased sintering and decreased surface area.

The TEM, SAED, and particle size studies show that Ni-Co-La/Al_2O_3 is the most effective catalyst for steam methane reforming. It is widely dispersed, crystalline, and thermally stable structure optimizes catalytic performance by reducing sintering while retaining a high hydrogen yield. This qualifies it as the most promising contender for industrial-scale methane reforming applications.

The TEM results are highly consistent with the BET (Brunauer-Emmett-Teller) surface area and pore structure studies shown in the table. The TEM micrographs show that Ni-Co-La/Al_2O_3 has the smallest and most uniformly dispersed nanoparticles, which aligns well with the BET data showing a moderately large surface area (83.44 m^2/g), moderate pore

volume (0.143 cm^3/g), and an ideal pore diameter (22.31 nm). These qualities help to improve catalytic performance by offering a high number of active sites and increasing mass transfer during steam methane reforming (SMR). XRD investigation yield a crystal size of 6.68 nm for Ni-Co-La/Al_2O_3, consistent with the small particle size reported in TEM (~9.47-13.97 nm). The presence of La stabilizes the metal nanoparticles, avoiding excessive development and sintering, as evidenced by the TEM images, which show well-dispersed and smaller particles.

Compared to Ni-Co-Fe/Al_2O_3, which has a lower surface area (64.34 m^2/g), larger pore diameter (29.46 nm), and slightly higher crystallite size (9.46 nm), TEM images show relatively larger and more aggregated particles, supporting the idea that this catalyst has lower dispersion and possibly lower long-term stability. Additionally, the spent catalysts (Ni-Co-La/Al_2O_3 and Ni-Co-Fe/Al_2O_3) show reduced surface area and increased particle size, indicating sintering and possible carbon deposition. But no carbon deposition is observed in the TEM images, it concludes sintering effect in the particles. Spent Ni-Co-La/Al_2O_3 has a higher surface area (77.02 m^2/g) and smaller crystal size (7.58 nm) than spent Ni-Co-Fe/Al_2O_3 (55.34 m^2/g, 9.34 nm), indicating that the catalyst is more resistant to deactivation. TEM, SAED, particle size distribution, and BET studies all corroborate the conclusion that Ni-Co-La/Al_2O_3 is the optimum catalyst for steam methane reforming. Its large surface area, tiny particle size, evenly distributed nanoparticles, and stable pore structure all contribute to excellent catalytic performance and long-term durability. The addition of La stabilizes the metal-support interaction, reduces sintering, and prevents coke formation, making Ni-Co-La/Al_2O_3 the most promising catalyst for SMR applications.[56]

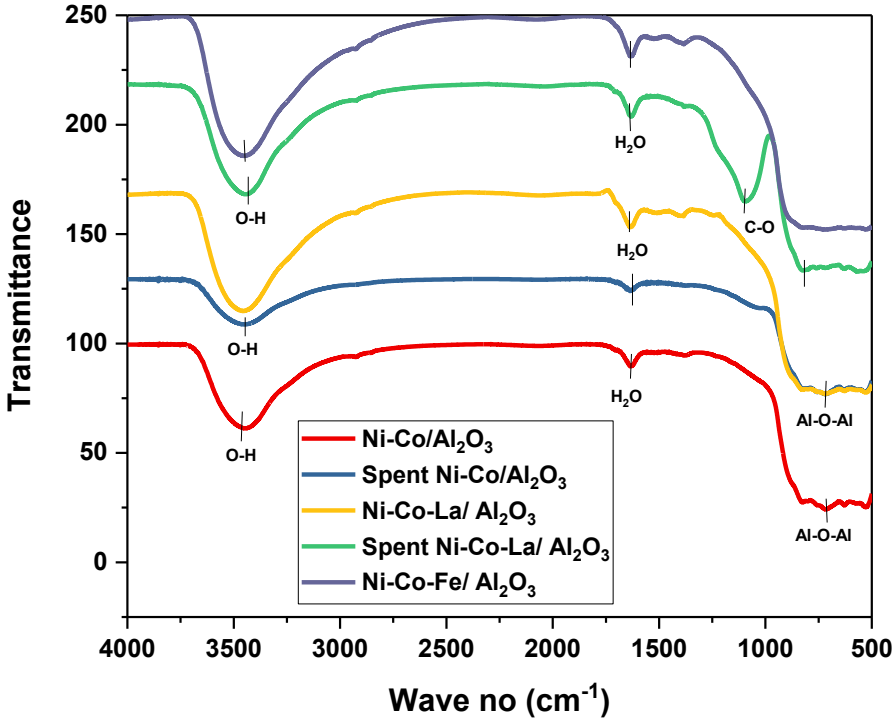

Fig. 5.19 FTIR analysis of synthesized catalysts

Fig 5.19 represents the FTIR (Fourier transform infrared spectroscopy) analysis which indicated different functional groups present in alumina-based catalyst in the range of 500-4000cm^{-1}. The broad peak observed at wave no 3400- 3500cm^{-1} represents O-H bond stretching in fresh catalyst of Ni-Co/Al_2O_3 [56] The valley from 1000-500cm^{-1} indicates Al_2O_3 structure while an intense peak was observed at 1500-1800cm^{-1} which corresponds to adsorption of H_2O on the catalyst surface. The shoulder peak was also observed at 867cm^{-1} which indicated the Al-O-Al vibrational peak. According to the literature, the peak in the range of 500-700cm^{-1} associated with octahedral AlO_6 sites while peaks generated in the range of 700-900cm^{-1} corresponds to tetrahedral AlO_4 sites. [71, 72] The associated with 800cm^{-1} associated with both tetrahedral and octahedral Al_2O_3.

5.6.2 Catalytic activity of steam methane reforming

Monometallic and bimetallic catalyst of cobalt supported on alumina and ceria supports were already tested to check best support in terms of conversion and stability of catalyst in chapter 4, Fig. 4.9. The catalyst deactivation was observed in ceria-based catalysts in both monometallic and bimetallic catalyst. Therefore, catalyst supported on alumina showed good activity as compared to ceria-supported catalyst.

And it can be observed that the Ni-Co combination played a great role in influencing the catalytic activity. It achieved a good conversion with no deactivation of catalyst for 1 hour of study. But Ni-Co combination also showed decline in catalytic activity after 12 hours of study as literature already reported. Lanthanum and iron as promoters used to promote the water gas shift reaction to lowering down the CO selectivity and converting the CO to CO_2 by enhancing the water gas shift reaction [73]. Moreover, CO_2 selectivity is low at higher temperatures. Therefore, to get the lower CO selectivity even at higher temperatures, the addition of iron and lanthanum was done with the combination of Ni-Co. Therefore, the combination of Ni-Co with addition of lanthanum and iron was tested for the steam methane reforming to get the maximum conversion by lowering the CO selectivity with no coke deposition is tested in this chapter as shown in Fig 5.20.

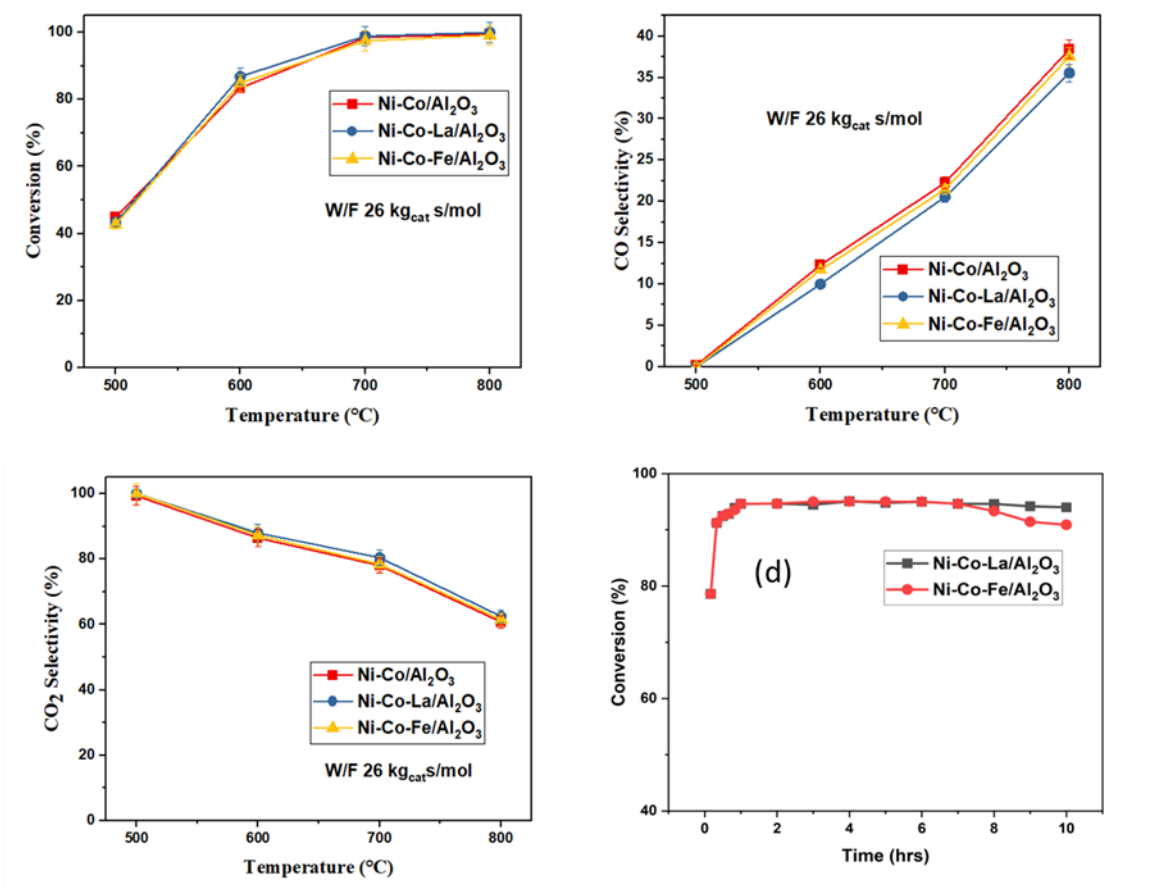

Fig. 5.20 (a) conversion vs temperature graph of all alumina supported catalysts (b) CO selectivity vs temperature graph (c) CO_2 selectivity vs temperature graph (d) Conversion vs temperature graph of both trimetallic catalysts at 700°C

Fig 5.20 shows the catalytic performance of trimetallic catalyst Ni-Co-La/Al_2O_3 and Ni-Co-Fe/Al_2O_3 catalyst. As can be seen, both iron and lanthanum showed good catalytic performance as compared to bimetallic Ni-Co/Al_2O_3. But lanthanum as a promoter lowers the CO selectivity at higher temperatures also. whereas, from Fig 5.20(d), conversion for both trimetallic catalysts was observed with lanthanum and iron both as promoters. Ni-Co-La/Al_2O_3 was also observed to lower the start-up time of the reaction. Ni-Co-Fe/Al_2O_3 showed decline in catalyst activity after 7 hours of study but Ni-Co-La/Al_2O_3 showed constant conversion throughout the study. Therefore, it can be concluded that the trimetallic catalyst Ni-Co-La/Al_2O_3 showed promising results for steam methane reforming [74].

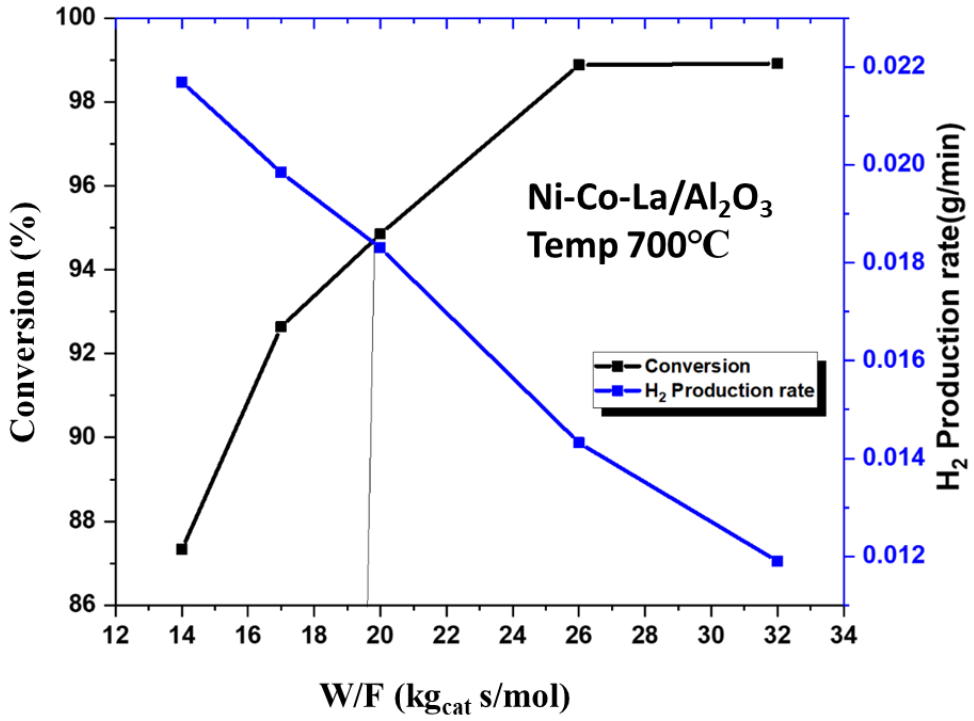

Fig. 5.21 Conversion, H_2 production rate vs W/F graph of Ni-Co-La/Al_2O_3 catalyst

Fig. 5.21 shows the graph of conversion vs hydrogen production rate by varying W/F value (W represents the weight of the catalyst and F is molar rate of methane). It was observed from graph that conversion is directly proportional to the W/F value [75]. Moreover, the Hydrogen production rate is inversely proportional to W/F value. It can be concluded from the graph that as conversion is increasing, the hydrogen production rate decreases. Therefore, there is a need to find an optimum value where these two lines in the graph crossed to each other. The conversion line and hydrogen production rate crossed to each other at W/F 19.5kg_{cat}s/mol. Hence W/F 19.5kg_{cat}s/mol was chosen as the optimum value.

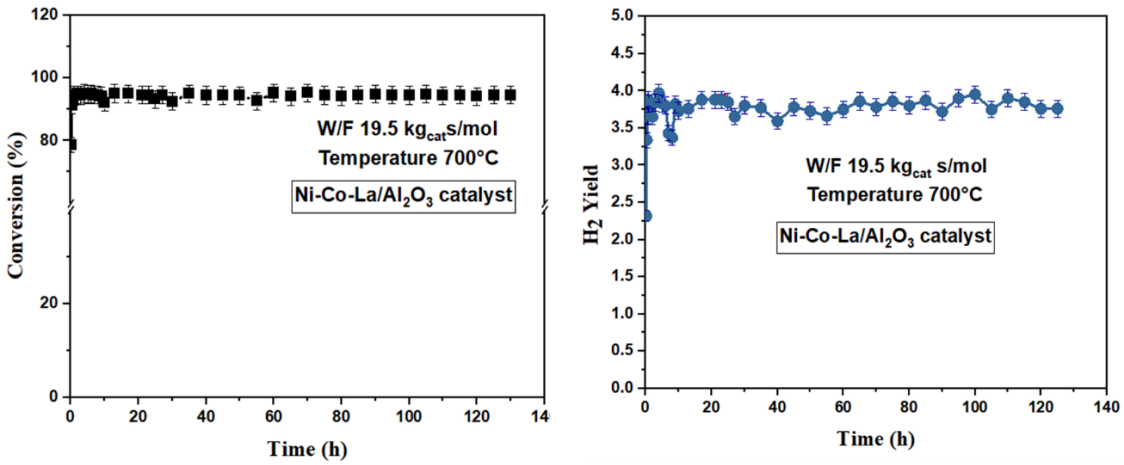

Fig. 5.22 Life cycle study of Ni-Co-La/Al_2O_3 catalyst

Fig 5.22 shows the conversion vs time graph of the Ni-Co-La/Al_2O_3 catalyst for almost 130 hours. The life cycle study of the Ni-Co-La/Al_2O_3 catalyst was tested at optimum conditions of reaction (W/F 19.5 kg_{cat}s/mol, temperature 700°C). This catalyst was stable for more than 130 hours with a constant conversion of 95% at 700°C. Similarly, Fig 5.22 (b) shows the Hydrogen Yield vs time graph of the Ni-Co-La/Al_2O_3 catalyst for more than 130 hours. As we can see from this graph hydrogen yield (~3.8) was also constant. Therefore, this could be a result of the addition of lanthanum as a promoter with Ni-Co combination. Zolghadri et al. [76] reported the stability of Ni-Co/Al_2O_3 catalyst. They concluded that due to coke deposition, the catalytic activity of the catalyst was reduced after 12 hours. But in this work, Ni-Co-La/Al_2O_3 shows outstanding performance in terms of stability with the addition of lanthanum as shown in Fig 5.22 [77]. Lanthanum helps to reduce agglomeration or sintering of catalyst at high temperature which can be confirmed with SEM and TEM analysis which could be attributed to high stability of Ni-Co-La/Al_2O_3.

Effect of S/M ratio

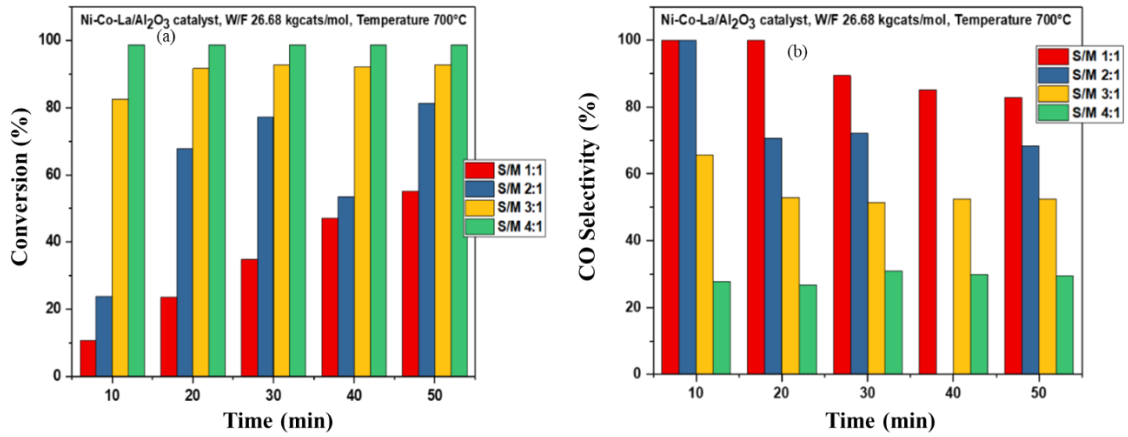

Fig. 5.23 Conversion vs time graph of Ni-Co-La/Al_2O_3 at different S/M ratios

Fig 5.23 shows effect of S/M ratio of Ni-Co-La/Al_2O_3 catalyst at 10% metal loading. The effect of molar ratio was studied by varying S/M ratio from 1:1 to 4:1 at temperature 700°C, W/F 26.68 $kg_{cat}s$/mol. It is observed from the graph that methane conversion is increasing by increasing S/M ratio. Increased in S/M ratio from 1:1 to 4:1 has significantly increased the conversion from 55% to 99%. CO selectivity gets reduced by increasing S/M ratio. The effect of S/M ratio on H_2 recovery is remarkable at these reaction conditions. Figure shows that an optimum value of S/M ratio is required. Hence it can be concluded that optimum value of S/M ratio is 1:4 with maximum conversion. The maximum conversion achieved at S/M ratio 4:1 is (~100%). These results are in agreement with the methane conversion obtained by chibane and Djellouli [78]. According to Le-Chatelier principle, increasing S/M ratio will shift the equilibrium towards CO_2 formation which will reduce the CO selectivity. Increasing steam improves interaction between CO molecule and steam by increasing reaction rate by converting CO into CO_2.

5.7 Comparison of trimetallic catalysts to be used for upscaling

Significant variations in catalytic performance are found when the three trimetallic catalysts for steam methane reforming Ni-Co-La/Al_2O_3, Ni-Co-Fe/Al_2O_3, and Ni-Fe-La/Al_2O_3 are compared as shown in Fig 5.24.

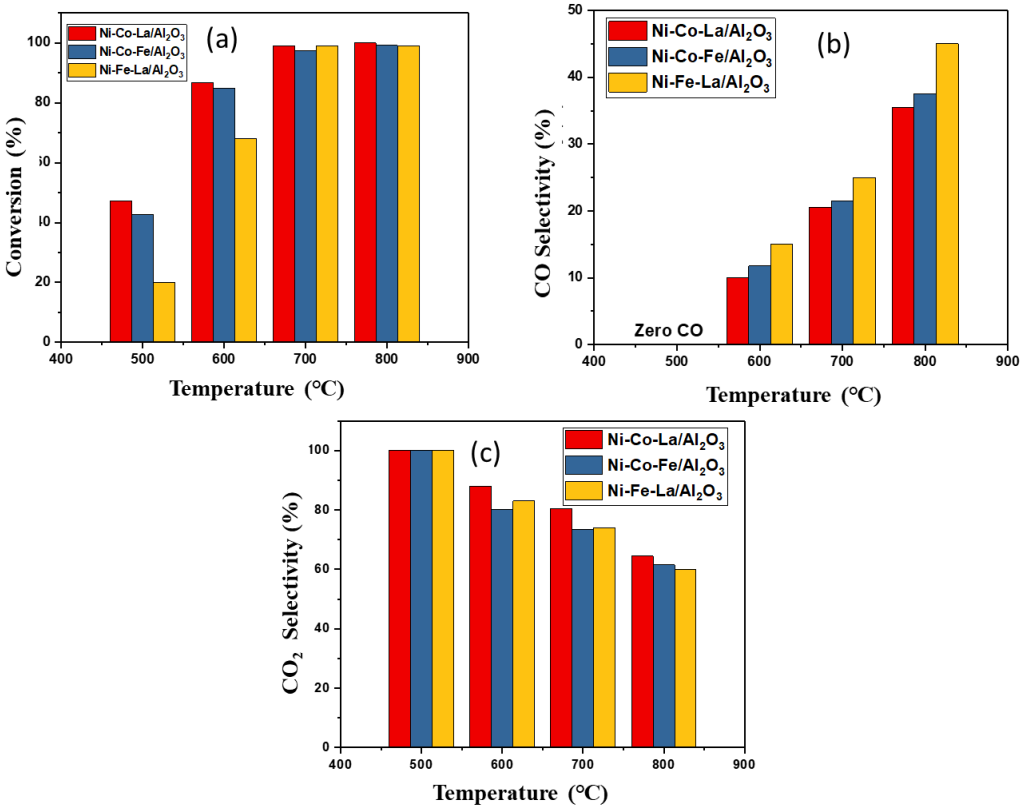

Fig. 5.24 Comparison of all trimetallic catalysts (a) Conversion graph (b) CO selectivity graph (c) CO_2 selectivity

For all catalysts, methane conversion rises with temperature; nevertheless, Ni-Co-La/Al_2O_3 and Ni-Co-Fe/Al_2O_3 show higher conversion rates than Ni-Fe-La/Al_2O_3. All catalysts get about 100% conversion at 800°C, demonstrating their potency at elevated temperatures. Ni-Fe-La/Al_2O_3 has the highest CO selectivity values, followed by Ni-Co-Fe/Al_2O_3, while Ni-Co-La/Al_2O_3 has the lowest. This suggests that Ni-Co-La/Al_2O_3 promotes the water-gas shift (WGS) process, which lowers the amount of CO. Ni-Co-La/Al_2O_3 has the highest CO_2 selectivity, followed by Ni-Co-Fe/Al_2O_3 and Ni-Fe-La/Al_2O_3. This suggests that Ni-Co-

La/Al_2O_3 improves the WGS process, which makes it a better option for producing hydrogen with little CO contamination. Because of its high methane conversion, low CO selectivity, and high CO_2 selectivity, $Ni\text{-}Co\text{-}La/Al_2O_3$ is the most promising catalyst overall and can be used to produce hydrogen-rich syngas. Then this catalyst is tested for upscale studies in packed bed reactor of diameter 6.35 cm.

5.8 Conclusions

In order to achieve maximal methane conversion at low temperatures while minimizing CO selectivity, we effectively synthesized trimetallic catalysts- $Ni\text{-}Fe\text{-}La/Al_2O_3$, $Ni\text{-}Co\text{-}La/Al_2O_3$, and $Ni\text{-}Co\text{-}Fe/Al_2O_3$ for steam methane reforming (SMR) in this study. With the maximum methane conversion at lower temperatures and zero CO selectivity, $Ni\text{-}Co\text{-}La/Al_2O_3$ outperformed the other catalysts in the test. This catalyst matched the intended performance parameters and demonstrated a great deal of promise for increasing the reforming process efficiency. Because of these results, this catalyst will be the subject of upscaling experiments, in which its performance will be assessed under more industrially relevant circumstances in a larger-scale reactor (Internal diameter: 6.35 cm). As our objective of getting maximum conversion at low temperature with minimum CO selectivity, only trimetallic catalyst fulfills it by getting maximum conversion and zero CO selectivity at 500℃. Although the CO selectivity is 18% at 500℃ for monometallic Ni/Al_2O_3 and Ni/CeO_2 catalyst and reduced to 6% for bimetallic catalyst (Ni-Fe) and 18% for bimetallic catalyst (Ni-La). Ni-Co based bimetallic catalyst getting Zero CO selectivity at 500℃ but this catalyst is deactivating after 12 hours of study. Therefore, all trimetallic catalyst have been tested in small reactor of I.D 11.74mm and results showed that trimetallic catalyst is showing good conversion at 500℃ with zero CO selectivity. This catalyst is also tested for long term stability test. There is no deactivation of trimetallic catalyst for at least 130 hours. It is observed that Ni: Co: La based catalyst exhibited

superior catalytic activity in terms of conversion, selectivity, and long-term stability in packed bed reactor of diameter 11.74mm. Therefore, in chapter 6, this catalyst synthesized in bulk and tested in large reactor of I.D 6.35cm. However, during large scale experiments, several challenges may be encountered including heat and mass transfer limitation, and process conditions. However, our objective of getting maximum conversion at low temperature (500°C) with reduced CO selectivity in large scale reactor.

References

1. Agnelli, M. E., Ponzi, E. N., Demicheli, M. C. (1987). Catalytic deactivation of methane steam reforming catalysts. *Industrial & engineering chemistry research*, 26(8), 1704-1707.
2. Hashemnejad, S. M., Parvari, M. (2011). Deactivation and regeneration of nickel-based catalysts for steam-methane reforming. *Chinese Journal of catalysis*, 32(1-2), 273-279.
3. Trimm, D. L. (1997). Coke formation and minimisation during steam reforming reactions. *Catalysis Today*, 37(3), 233-238.
4. Kusakabe, K., Sotowa, K. I., Eda, T., Iwamoto, Y. (2004). Methane steam reforming over Ce–ZrO_2-supported noble metal catalysts at low temperature. *Fuel Processing Technology*, 86(3), 319-326.
5. Li, D., Nakagawa, Y., Tomishige, K. (2011). Methane reforming to synthesis gas over Ni catalysts modified with noble metals. *Applied Catalysis A: General*, 408(1-2), 1-24.
6. Nieva, M. A., Villaverde, M. M., Monzón, A., Garetto, T. F., Marchi, A. J. (2014). Steam-methane reforming at low temperature on nickel-based catalysts. *Chemical Engineering Journal*, 235, 158-166.
7. Wu, H., La Parola, V., Pantaleo, G., Puleo, F., Venezia, A. M., Liotta, L. F. (2013). Ni-based catalysts for low temperature methane steam reforming: recent results on Ni-Au and comparison with other bi-metallic systems. *Catalysts*, 3(2), 563-583.
8. Pistonesi, C., Juan, A., Irigoyen, B., Amadeo, N. (2007). Theoretical and experimental study of methane steam reforming reactions over nickel catalyst. *Applied surface science*, 253(9), 4427-4437.

9. Baudh, A., Sharma, R., Sharma, S., Kumar Upadhyay, R. (2024). Effect of Lanthanum and Iron Doping on Nickel-Based Alumina and Ceria Supported Catalysts for Steam Reforming of Methane. *ChemistrySelect*, 9(19), e202401393.
10. You, X., Wang, X., Ma, Y., Liu, J., Liu, W., Xu, X., Chen, X. (2014). Ni–Co/Al_2O_3 bimetallic catalysts for CH_4 steam reforming: elucidating the role of Co for improving coke resistance. *ChemCatChem*, 6(12), 3377-3386.
11. Braga, A., Armengol-Profitós, M., Pascua-Solé, L., Vendrell, X., Soler, L., Serrano, I., Llorca, J. (2023). Bimetallic NiFe Nanoparticles Supported on CeO_2 as Catalysts for Methane Steam Reforming. *ACS applied nano materials*, 6(9), 7173-7185.
12. Torimoto, M., Ogo, S., Hisai, Y., Nakano, N., Takahashi, A., Ma, Q., Sekine, Y. (2020). Support effects on catalysis of low temperature methane steam reforming. *RSC advances*, 10(44), 26418-26424.
13. Mei, D., Glezakou, V. A., Lebarbier, V., Kovarik, L., Wan, H., Albrecht, K. O., Dagle, R. A. (2014). Highly active and stable $MgAl_2O_4$ supported Rh and Ir catalysts for methane steam reforming: A combined experimental and theoretical study. *Journal of Catalysis*, 316, 11-23.
14. Ligthart, D. M., Pieterse, J. A., Hensen, E. J. (2011). The role of promoters for Ni catalysts in low temperature (membrane) steam methane reforming. *Applied Catalysis A: General*, 405(1-2), 108-119.
15. Maluf, S. S., Assaf, E. M. (2009). Ni catalysts with Mo promoter for methane steam reforming. *Fuel*, 88(9), 1547-1553.
16. Jakobsen, J. G., Jakobsen, M., Chorkendorff, I., Sehested, J. (2010). Methane steam reforming kinetics for a rhodium-based catalyst. *Catalysis letters*, 140, 90-97.
17. Didenko, L. P., Sementsova, L. A., Chizhov, P. E., Dorofeeva, T. V. (2019). Steam reforming of methane and its mixtures with propane in a membrane reactor with

industrial nickel catalyst and palladium–ruthenium foil. *Petroleum Chemistry*, 59, 394-404.

18. Ligthart, D. M., Pieterse, J. A., Hensen, E. J. (2011). The role of promoters for Ni catalysts in low temperature (membrane) steam methane reforming. *Applied Catalysis A: General*, 405(1-2), 108-119.
19. Hu, Z., Miao, Z., Wu, J., Jiang, E. (2021). Nickel-iron modified natural ore oxygen carriers for chemical looping steam methane reforming to produce hydrogen. *International Journal of Hydrogen Energy*, 46(80), 39700-39718.
20. Al-Fatesh, A. S., Patel, N., Srivastava, V. K., Osman, A. I., Rooney, D. W., Fakeeha, A. H., Kumar, R. (2025). Iron-promoted zirconia-alumina supported Ni catalyst for highly efficient and cost-effective hydrogen production via dry reforming of methane. *journal of environmental sciences*, 148, 274-282.
21. Boudjeloud, M., Boulahouache, A., Rabia, C., Salhi, N. (2019). La-doped supported Ni catalysts for steam reforming of methane. *International journal of hydrogen energy*, 44(20), 9906-9913.
22. Lara, T. P., Petrolini, D. D., de Oliveira Rocha, K., dos Santos, J. B., Bueno, J. M. (2024). In situ study of structural modifications in Ni-Fe/MgAl2O4 catalysts employed for ethanol steam reforming. *Fuel*, *373*, 132336.
23. Shah, S., Hong, J., Cruz, L., Wasantwisut, S., Bare, S. R., Gilliard-AbdulAziz, K. L. (2023). Dynamic tracking of NiFe smart catalysts using in situ X-ray absorption spectroscopy for the dry methane reforming reaction. *ACS Catalysis*, *13*(6), 3990-4002.
24. Shah, M., Al Mesfer, M. K., Danish, M. (2023). Design and optimization of Ni–Fe–La based catalytic system for CO_2 utilization for sustainable syngas production via dry reforming of methane. *Journal of the Energy Institute*, *110*, 101346.

25. Isupova, L. A., Ivanova, Y. A., Prosvirin, I. P., Gerasimov, E. Y. (2024). LaFe 1−x Ni x O_3 perovskites in the catalytic reaction of high-temperature decomposition of nitrous oxide. *Dalton Transactions*, *53*(36), 15273-15283.
26. Sarmad, Q., Khan, U. M., Anwar, M., Khoja, A. H., Ali, M., Khan, Z. S., Somalu, M. R. (2021). Catalytic Performance of Calcium-Lanthanum co-doped Ceria (Ce0.85-xLa0. 15CaxO_2-δ) in Partial Oxidation of Methane. *Bulletin of Chemical Reaction Engineering & Catalysis*, *16*(3), 548-554.
27. Manabayeva, A. M., Mäki-Arvela, P., Vajglová, Z., Martinéz-Klimov, M., Tirri, T., Baizhumanova, T. S., Tungatarova, S. A. (2023). Dry Reforming of Methane over Ni–Fe–Al Catalysts Prepared by Solution Combustion Synthesis. *Industrial & Engineering Chemistry Research*, 62(29), 11439-11455.
28. Wu, Y., Pei, C., Tian, H., Liu, T., Zhang, X., Chen, S., Gong, J. (2021). Role of Fe species of Ni-based catalysts for efficient low-temperature ethanol steam reforming. *Jacs Au,* 1(9), 1459-1470.
29. Xu, J., & Froment, G. F. (1989). Methane steam reforming, methanation and water-gas shift: I. Intrinsic kinetics. *AIChE journal*, 35(1), 88-96.
30. Iglesia, E. (1997). Design, synthesis, and use of cobalt-based Fischer-Tropsch synthesis catalysts. *Applied Catalysis A: General*, 161(1-2), 59-78.
31. Chen, M., Wang, L. (2024). Performance of Ni-Based Catalysts with La Promoter for the Reforming of Methane in Gasification Process. *Catalysts*, 14(6), 355.
32. Biesinger, M. C., Payne, B. P., Grosvenor, A. P., Lau, L. W., Gerson, A. R., Smart, R. S. C. (2011). Resolving surface chemical states in XPS analysis of first row transition metals, oxides and hydroxides: Cr, Mn, Fe, Co and Ni. *Applied Surface Science*, 257(7), 2717-2730.

33. Chastain, J., & King Jr, R. C. (1992). Handbook of X-ray photoelectron spectroscopy. *Perkin-Elmer Corporation*, 40, 221.

34. Wei, Y., Song, M., Yu, L., & Meng, F. (2021). CO_2 reforming of methane over carbon fiber-lanthanum oxide supported bimetallic nickel-cobalt catalysts: Kinetic and mechanistic studies. *Process Safety and Environmental Protection*, 145, 236-246.

35. Al-Ubaid, A.,Wolf, E. E. (1987). Activity, FTIR studies and catalyst characterization during methane steam reforming on Ni/Y-zeolite catalysts. *Applied catalysis*, 34, 119-134.

36. Morlanés, N. (2013). Reaction mechanism of naphtha steam reforming on nickel-based catalysts, and FTIR spectroscopy with CO adsorption to elucidate real active sites. *International journal of hydrogen energy*, 38(9), 3588-3596.

37. Parizotto, N. V., Rocha, K. O., Damyanova, S., Passos, F. B., Zanchet, D., Marques, C. M. P., Bueno, J. M. C. (2007). Alumina-supported Ni catalysts modified with silver for the steam reforming of methane: effect of Ag on the control of coke formation. *Applied Catalysis A: General*, 330, 12-22.

38. King, D. L., Strohm, J. J., Wang, X., Roh, H. S., Wang, C., Chin, Y. H , Singh, P. (2008). Effect of nickel microstructure on methane steam-reforming activity of Ni–YSZ cermet anode catalyst. *Journal of Catalysis*, 258(2), 356-365.

39. Hashemnejad, S. M., Parvari, M. (2011). Deactivation and regeneration of nickel-based catalysts for steam-methane reforming. *Chinese Journal of catalysis*, 32(1-2), 273-279.

40. Sabirova, Z. A., Danilova, M. M., Zaikovskii, V. I., Kuzin, N. A., Kirillov, V. A., Kriger, T. A., Khrobostov, L. N. (2008). Nickel catalysts based on porous nickel for methane steam reforming. *Kinetics and Catalysis*, 49, 428-434.

41. Noronha F B.(2008) Effect of CeO_2 and La_2O_3 on the Activity of CeO_2–La_2O_3/Al_2O_3-Supported Pd Catalysts for Steam Reforming of Methane.
42. Wu H, La Parola V, Pantaleo G, Puleo F, Venezia A M, Liotta L F. (2013) Ni-based catalysts for low temperature methane steam reforming: recent results on Ni-Au and comparison with other bi-metallic systems. *Catalysts*, 3(2): 563-583.
43. Soloviev S O, Gubareni I V, Orlyk S M.(2018) Oxidative reforming of methane on structured nickel–alumina catalysts: a review. *Theoretical and Experimental Chemistry*, 54, 293-315.
44. Yu, J., Le, T., Jing, D., Stavitski, E., Hunter, N., Lalit, K., Huang, W. (2023). Balancing elementary steps enables coke-free dry reforming of methane. Nature communications, 14(1), 7514.
45. Da Silva, A. L., Den Breejen, J. P., Mattos, L. V., Bitter, J. H., De Jong, K. P., Noronha, F. B. (2014). Cobalt particle size effects on catalytic performance for ethanol steam reforming–Smaller is better. *Journal of catalysis*, 318, 67-74.
46. Philia, J., Widayat, W., & Sulardjaka, S. (2023). hydrogen production from ethanol by steam reforming over nickel and cobalt geothermal waste supported catalyst. Rasayan *Journal of Chemistry*, 16(1)
47. Seman M H A, Othman N H, Osman N, Jani A M M. Nickel based catalysts supported on porous support for methane steam reforming: potential and short review. In *IOP Conference Series: Earth and Environmental Science* 2023; 1151.
48. Al Abdulghani, A. J., Park, J. H., Kozlov, S. M., Kang, D. C., Al Sabban, B., Pedireddy, S., Takanabe, K. (2020). Methane dry reforming on supported cobalt nanoparticles promoted by boron. *Journal of catalysis*, 392, 126-134.

49. Ayodele, B. V., Khan, M. R., Cheng, C. K. (2015). Syngas production from CO_2 reforming of methane over ceria supported cobalt catalyst: Effects of reactants partial pressure. *Journal of Natural Gas Science and Engineering*, 27, 1016-1023.
50. Da Costa-Serra, J., Guil-Lopez, R.,Chica, A. (2010). Co/ZnO and Ni/ZnO catalysts for hydrogen production by bioethanol steam reforming. Influence of ZnO support morphology on the catalytic properties of Co and Ni active phases. *International Journal of Hydrogen Energy*, 35(13), 6709-6716.
51. Reddy B M, Rao K N, Bharali P. (2009) Copper promoted cobalt and nickel catalysts supported on ceria− alumina mixed oxide: Structural characterization and CO oxidation activity. *Industrial & engineering chemistry research*, 48(18), 8478-8486.
52. Profeti L P, Ticianelli E A, Assaf E M. (2008) Co/Al_2O_3 catalysts promoted with noble metals for production of hydrogen by methane steam reforming. *Fuel*, 87,10-11,2076-2081.
53. Ishihara, A., Tsujino, H., Hashimoto, T. (2021). Effects of the addition of CeO_2 on the steam reforming of ethanol using novel carbon-Al_2O_3 and carbon ZrO_2 composite-supported Co catalysts. *RSC advances*, 11(15), 8530-8539.
54. Boudjeloud M, Boulahouache A, Rabia C, Salhi N. (2019) La-doped supported Ni catalysts for steam reforming of methane. *International journal of hydrogen energy*, 44(20), 9906-9913.
55. Hu Z, Miao Z, Wu J, Jiang E. (2021) Nickel-iron modified natural ore oxygen carriers for chemical looping steam methane reforming to produce hydrogen. *International Journal of Hydrogen Energy*; 46(80): 39700-39718.
56. Zarei-Jelyani F, Salahi F, Farsi M, Rahimpour M R. (2022) Synthesis and application of Ni-Co bimetallic catalysts supported on hollow sphere Al_2O_3 in steam methane reforming. *Fuel*, 324, 124785.

57. Shafiee, P., Alavi, S. M., Rezaei, M., amp; Jokar, F. (2022). Promoted Ni–Co/Al_2O_3 nanostructured catalysts for CO_2 methanation. International Journal of Hydrogen Energy, 47(4), 2399-2411.

58. Romero C, L., Moreno, M. S., Galetti, A. E., Barroso, M. N. (2022). Ni–Co bimetallic catalysts for hydrogen production by steam reforming ethanol. *Topics in Catalysis*, 65(13), 1427-1439.

59. Deng, Y., Jeong, M. H., Park, K. S., Bae, J. W. (2025). Chemical-looping-based syngas production by separate CH_4 decomposition and CO_2 activation over mesoporous Ni-Co/MgAl2O4. *Chemical Engineering Journal*, 160351.

60. Pachatouridou, E., Zeza, E., Lappas, A., Iliopoulou, E. (2025). Study of Co/γ-Al2O3 and Fe/γ-Al2O3 materials for catalytic methane pyrolysis to CO2-free hydrogen. *International Journal of Hydrogen Energy*, *101*, 785-796.

61. Mageed, A. K., Alsaffar, M. A., Ghany, M. A. R. A., Sukkar, K. A., Ayodele, B. V. (2024). Advances in synthesis and application of cobalt and nickel-based nanomaterials for catalytic reforming of hydrocarbons and oxygenates to hydrogen-rich syngas. *Journal of Industrial and Engineering Chemistry*.

62. Baudh, A., Sharma, R., Sharma, S., Kumar Upadhyay, R. (2024). Effect of Lanthanum and Iron Doping on Nickel-Based Alumina and Ceria Supported Catalysts for Steam Reforming of Methane. *ChemistrySelect*, *9*(19), e202401393.

63. Ay H, Üner D. (2015) Dry reforming of methane over CeO_2 supported Ni, Co and Ni–Co catalysts. *Applied Catalysis B: Environmental*, 179, 128-138.

64. Ding X, Li B, Yang Y, Liu X, Guo Y, Wang Y. (2024) Steam reforming of methane over nickel-aluminum spinel-derived catalyst. *International Journal of Hydrogen Energy*, 51,1256-1266.

65. Guo S, Sun Y, Zhang Y, Zhang C, Li Y, Bai J. (2024) Bimetallic Nickel-Cobalt catalysts and their application in dry reforming reaction of methane. Fuel, 358, 130290.

66. Ou Z, Ran J, Qiu H, Huang X, Qin C. (2024) Understanding the role of Co segregation on the carbon deposition over Ni–Co bimetal catalyst in dry reforming of methane. *Separation and Purification Technology*, 333, 125868.

67. Panda S, Joshi V, Shrivastaw V K, Das S, Poddar M, Bal R, Bordoloi A. (2023) Enhanced coke-resistant Co-modified Ni/modified alumina catalyst for the bireforming of methane. *Catalysis Science & Technology*, 13(15), 4506-4516.

68. Du, X., Zhang, D., Shi, L., Gao, R., Zhang, J. (2013). Coke-and sintering-resistant monolithic catalysts derived from in situ supported hydrotalcite-like films on Al wires for dry reforming of methane. *Nanoscale*, *5*(7), 2659-2663.

69. Trimm, D. L. (1977). The formation and removal of coke from nickel catalyst. *Catalysis Reviews Science and Engineering*, *16*(1), 155-189.

70. You, X., Wang, X., Ma, Y., Liu, J., Liu, W., Xu, X., Chen, X. (2014). Ni–Co/Al_2O_3 bimetallic catalysts for CH_4 steam reforming: elucidating the role of Co for improving coke resistance. *ChemCatChem*, *6*(12), 3377-3386.

71. Maldonado C S, Rosa J R, Lucio-Ortiz C J, Hernández-Ramírez A, Barraza F F C and Valente J S (2014) 'Low concentration Fe-Doped alumina catalysts using sol-gel and impregnation methods: the synthesis, characterization and catalytic performance during the combustion of trichloroethylene. *Materials,* 7, 2062–86

72. Paglia G, Buckley C E, Udovic T J, Rohl A L, Jones F, Maitland C F and Connolly J (2004) Boehmite-derived γ-alumina system consideration of hydrogen and surface effects Chem. *Mater.* 16 1914–23

73. Wang S, Nabavi S A, Clough P T. (2023) A review on bi/polymetallic catalysts for steam methane reforming. *international journal of hydrogen energy*.

74. Tran N T, Van Le Q, Van Cuong N, Nguyen T D, Phuc N H H, Phuong P T, Vo D V N (2020). La-doped cobalt supported on mesoporous alumina catalysts for improved methane dry reforming and coke mitigation. *Journal of the Energy Institute*, 93(4), 1571-1580.

75. Abbas S Z, Dupont V, Mahmud T. (2017) Kinetics study and modelling of steam methane reforming process over a NiO/Al_2O_3 catalyst in an adiabatic packed bed reactor. *International journal of hydrogen Energy*, 42(5), 2889-2903.

76. Zolghadri S, Honarvar B, Rahimpour M R. (2023) Synthesis, application, and characteristics of mesoporous alumina as a support of promoted Ni-Co bimetallic catalysts in steam reforming of methane. *Fuel*, 335, 127005.

77. You X, Wang X, Ma Y, Liu J, Liu W, Xu X, Chen, X. (2014) $Ni–Co/Al_2O_3$ bimetallic catalysts for CH_4 steam reforming: elucidating the role of Co for improving coke resistance. *ChemCatChem*, 6(12), 3377-3386.

78. Chibane L, Djellouli B. (2011) Methane steam reforming reaction behavior in a packed bed membrane reactor. *International Journal of Chemical Engineering and Applications*, 2(3), 147.